Joint Centre for Mesoscale Meteorology, Reading, UK

Attribution and its application to mesoscale structure associated with tropopause folds

A. J. Thorpe

Internal Report No. 73

September 1997

Met Office Joint Centre for Mesoscale Meteorology Department of Meteorology
University of Reading PO Box 243 Reading RG6 6BB United Kingdom
Tel: +44 (0)118 931 8425 Fax: +44 (0)118 931 8791
www.metoffice.com

Designed and produced by the Met Office © Crown copyright 2001 01/0240 The Met Office logo is a registered trademark.

Q. J. R. Meteorol. Soc. (1997), 123, pp. 1–16

Attribution and its application to mesoscale structure associated with tropopause folds

By A. J. THORPE *

Department of Meteorology, University of Reading

(Received 7 Sept 1996; revised 14 April 1997)

SUMMARY

It is important in meteorology to be able to establish a link between various features. This link in its strongest form would be referred to as "cause-and-effect" but this is extremely difficult to establish for atmospheric flows. A weaker, but nonetheless powerful, link is "attribution" which attempts to provide a way to associate various fundamental features such as potential vorticity anomalies to weather events involving regions of ascent. Attribution is not new and it is implicit in the way that atmospheric evolution is usually described. In this paper an attempt is made to define more precisely what are the steps and assumptions being made in such a method. These ideas become more concrete by applying them to a simple model of a two-dimensional front at which there is a tropopause fold. The aim is to find the vertical motion attributable to the descended tropopause fold in an extra-tropical cyclone. This is the first step in a longer programme of research designed to provide a test of the hypothesis that such a descended tropopause can trigger mesoscale phenomena such as convection and cyclones.

KEYWORDS: Forecasting Tropopause Attribution

1. INTRODUCTION

Both in forecasting and in research, understanding the evolution of weather events plays a central role. Understanding usually implies breaking down the complexity of the atmosphere to simpler building blocks encompassed in a theory. This theory often involves a simplified set of equations purporting to capture the essence of the process or phenomenon in question. Typically the theory is tested using data-sets, such as derived from atmospheric analyses, special field data or other (prediction) models, and such an application is referred to as diagnosis. There are many techniques involved in diagnosis, for example: lagged correlations, factor separation (Stein and Alpert 1993), EOF analysis etc.

For short periods, of up to perhaps 2 days ahead, deterministic concepts are still relevant, even noting the important advances in the theory of predictability and chaos, and so cause-and-effect is an attractive idea. In synoptic meteorology a question such as "did this upper-level trough trigger cyclogenesis?" is typical. Most diagnostic techniques rely on a partition of the atmosphere into parts which may interact with each other; for example, the use of the mean flow and perturbation in instability theories. Another partitioning, to be explored here, involves dividing the flow into potential vorticity anomalies and a background distribution of potential vorticity. Usually with such diagnostic techniques the most that can be said is that A (e.g. the cyclone in the previous example) is attributable to B (the trough) without implying that B causes A. However "attribution" is useful even without a firm cause-and-effect having been established.

Here attribution ideas are applied to potential vorticity thinking and their strengths and weaknesses are identified. For this the quasi-geostrophic and semi-geostrophic theories are used. This notion of attribution is not new and, for example, the papers of Davis and Emanuel (1991) and Davis (1992) develop ideas of piecewise potential vorticity inversion using the non-linear balance equations. Our aim here is to draw together these ideas using the simplest possible framework, namely the quasi-geostrophic model.

* Corresponding author: Department of Meteorology, University of Reading, Earley Gate, PO Box 243, Reading RG6 6BB, UK.

Specifically we wish to state precisely the steps and assumptions needed to find the vertical motion attributable to a potential vorticity anomaly. The reason this is an important problem is that potential vorticity is one of the most fundamental properties of a given flow, bearing in mind its conservation and inversion properties, and the understanding of vertical motion tells the forecaster much about the generation of weather elements. To explore the general aspects of attribution for this problem it is clearest to use the quasi-geostrophic model; see section 2.

Then the attribution method will be used to examine an important unresolved problem in mesoscale dynamics, namely the role of a descending tropopause fold in an extratropical cyclone in the generation of mesoscale phenomena. There has been speculation about whether the narrow descending tropopause, which occurs as a cyclone deepens, is responsible for the generation of significant mesoscale sub-structure within that cyclone. Elucidating the dynamical meteorology of the tropopause fold is the main goal of this and companion papers. For an accurate description of vertical motion attributable to a tropopause fold we use the semi-geostrophic model; see sections 3, 4 and 5.

2. Attribution using the quasi-geostrophic model

The building blocks we will use here are those implied by the quasi and semi-geostrophic models. It is convenient to summarize schematically the model. The quasi-geostrophic (QG) theory has a particularly simple form for an atmosphere with uniform density using the Boussinesq approximation and height as the vertical coordinate. (Note that it is straightforward to extend the theory to include a reference density which varies with height and to use pressure as a vertical coordinate.) The theory is based on geostrophic and hydrostatic balance and it provides four equations composed of 2 pairs of equations. The vorticity and thermodynamic equations form one pair. From these equations the potential vorticity and omega equations can be derived. Together they form the second pair of equations. The first is the QG vorticity equation:

$$D_g(f+\zeta_g) = f_0 \frac{\partial w}{\partial z} \tag{1}$$

The definitions of these and other terms in this paper are given in the Appendix. Equation (1) shows that the main mechanism for the development of cyclonic systems (i.e. low-pressure centres) is the stretching of the Earth's vorticity. The second is the thermodynamic equation:

$$D_g b' = -wN^2 \tag{2}$$

This equation is derived from the conservation of potential temperature (i.e. dry adiabatic motion) and shows, for example, that as air rises it cools via adiabatic expansion. The third equation, derived by combining equations (1) and (2) is that for the potential vorticity:

$$D_g q = 0 \tag{3}$$

where q is the QG potential vorticity defined as $q = \mathcal{N}_1[\psi]$, where ψ is the geostrophic streamfunction and $\mathcal{N}_1$ is a second order differential operator defined in the Appendix. Equation (3) shows that in addition to the conservation of potential temperature the air conserves the QG potential vorticity if the motion is frictionless. Finally there is the omega equation obtained by eliminating the time derivatives between equations (1) and (2) using thermal wind balance:

$$\mathcal{N}_2 [w] = S = 2\nabla.\underline{Q} \tag{4}$$

This is a diagnostic equation, usually called the omega equation, which allows the vertical motion to be obtained knowing the forcing S which can be calculated directly from the pressure field or the streamfunction. Notice that $\mathcal{N}_2$ is a second order differential operator.

The model clearly places the vertical velocity and the potential vorticity at centre-stage in terms of the generation of vorticity. Thus two simple, and equivalent, ways to interpret synoptic development are:

- The current vorticity and thermal patterns evolve due to geostrophic advection and vertical motion. The new vorticity distribution implies a new flow from vorticity inversion. This together with the new temperature field imply a changed forcing of vertical motion. The new vertical motion can be obtained from the omega equation.
- The potential vorticity viewpoint allows a simplification in this interpretation. The current potential vorticity pattern evolves due to geostrophic advection alone. The new potential vorticity distribution implies a new flow and temperature from potential vorticity inversion. The new flow and temperature give a new forcing of vertical motion which, in turn, is obtained from the omega equation. Notice that the vertical motion is not explicitly needed to infer the evolution of the potential vorticity pattern.

The dynamical question posed here is which local features of the flow and temperature lead to localised regions of vertical motion associated with, or attributable to, a given synoptic system? This step is most elegantly achieved by the use of potential vorticity concepts. Given the conservation principle governing potential vorticity it is possible to regard the atmosphere as composed of a collection of pieces or anomalies of potential vorticity. Attribution then stems from the following schematic mathematically-described process. First divide the atmosphere into a potential vorticity anomaly (q') and the remaining, or "background", potential vorticity ($\overline{q}$), ie: $q = \overline{q} + q'$. (Discussion of how to define an anomaly and the background will be given later.) It is possible to invert the potential vorticity to obtain the geostrophic flow and temperature by solving the equation defining the potential vorticity. This is the invertibility principle and can be written symbolically as:

$$\psi = \mathcal{N}_1{}^{-1} [q] \tag{5}$$

where $\mathcal{N}_1{}^{-1}$ means solving the equation relating ψ and q assuming the distribution of q is known. This inversion is essentially the reverse process to the one by which the potential vorticity distribution is obtained from wind-field and temperature data. Given the partition of the potential vorticity field then the streamfunction can be similarly partitioned, ie: $\psi = \overline{\psi} + \psi'$. So the inversion of an individual potential vorticity anomaly can be obtained by taking the difference of the results of two inversions, one of the total potential vorticity and one of the background potential vorticity:

$$\psi' = \mathcal{N}_1{}^{-1} [q] - \mathcal{N}_1{}^{-1} [\overline{q}] \tag{6}$$

The interpretation of equation (6) is that ψ' is that part of the geostrophic flow and temperature attributable to the potential vorticity anomaly q'. As $\mathcal{N}_1$ is a linear operator for the QG theory then it is also true that $\psi' = \mathcal{N}_1{}^{-1} [q']$. Note that, even though $\mathcal{N}_1$ is a non-linear operator for higher-order balance assumptions, recent work suggests that this non-linearity may not be a large effect except very locally to the anomaly, Birkett and Thorpe 1997.

The omega equation (4) allows us to find the vertical motion attributable to the potential vorticity anomaly. First note that the forcing, on the right hand side of equation (4), can be written as $S = \mathcal{N}_3[\psi]$ (see equation (A.10) in the appendix) and that $\mathcal{N}_3$ is a non-linear function of ψ which means that $\mathcal{N}_3[\overline{\psi} + \psi'] \neq \mathcal{N}_3[\overline{\psi}] + \mathcal{N}_3[\psi']$. Also $\mathcal{N}_3$ is an implicit function of the potential vorticity. It is one of the aims of this paper to elucidate this function so as to provide some building blocks to allow vertical motion to be directly attributed to individual potential vorticity anomalies. The solution of the omega equation can be written symbolically as:

$$w = \mathcal{N}_2^{-1}[\mathcal{N}_3[\psi]] = \mathcal{N}_2^{-1}[\mathcal{N}_3[\mathcal{N}_1^{-1}[q]]] \tag{7}$$

This shows that vertical motion is associated with those potential vorticity distributions for which $\mathcal{N}_3[\mathcal{N}_1^{-1}[q]] \neq 0$. This is a special subset of all possible atmospheric distributions of potential vorticity. Using the same notation for the partitioning of the vertical velocity, $w = \overline{w} + w'$, allows the vertical motion attributable to a given potential vorticity anomaly to be written symbolically as:

$$w' = \mathcal{N}_2^{-1}[\mathcal{N}_3[\mathcal{N}_1^{-1}[q]]] - \mathcal{N}_2^{-1}[\mathcal{N}_3[\mathcal{N}_1^{-1}[\overline{q}]]] \tag{8}$$

Whilst in principle the procedure, implied by equation (8), is straightforward, in practice there are some important complications to be noted:

- The way to define an anomaly must be specified. A relatively simple way is to draw a surface in three-dimensional space around a particular region of potential vorticity. The anomaly then arises by subtracting from the potential vorticity in that region that value of potential vorticity typical of its immediate surroundings. Other possibilities are to use spatial or temporal averages. It is clear that attribution will give most insight if there is a scale separation between the anomaly and the background flow.
- A solution to equation (5) can only be obtained if suitable boundary conditions are provided. It is usual to specify θ at the boundaries which is equivalent to specifying the vertical gradient of ψ. It is possible to use other conditions such as on ψ itself and this choice remains as an arbitrariness in the results.
- Equation (6) can be simplified into a single inversion of q' if the operator $\mathcal{N}_1$ is linear. For the QG system it is linear but note that for more accurate approximations to the Ertel-Rossby potential vorticity, such as in the semi-geostrophic and non-linear balance systems, it is non-linear and two inversions are needed.
- Also the boundary conditions for each of the two inversions in Equation (6) must be determined. This requires a choice, again with arbitrariness, of partitioning the potential temperature at the boundary, *viz*: $\theta_b = \overline{\theta}_b + \theta_b'$. It is unclear how to make this decomposition although often it is assumed that $\theta_b' = 0$ so that there is no thermal anomaly at the surface attributable to the potential vorticity anomaly.
- Equations (7) and (8) require boundary conditions but over the oceans these are simply $w = 0$ at the surface and at the upper boundary if it is high enough, say above the tropopause.
- The non-linearity of $\mathcal{N}_3$ means that there is an alternative method to find w'. The method already described in equation (8) involves subtraction of the results of two inversions of the omega equation using the total potential vorticity and the background potential vorticity respectively. The alternative method is to obtain w' directly from the potential vorticity anomaly itself, via:

$$w' = \mathcal{N}_2^{-1}[\mathcal{N}_3[\mathcal{N}_1^{-1}[q']]] \tag{9}$$

The choice of whether to use equation (8) or equation (9) is unclear and their solutions will be different. The nature of this difference needs to be assessed.

Probably the most important aspect of this procedure to note is the non-linearity of the operator $\mathcal{N}_3$. Consider first using equation (8). It is straightforward to show that the non-linearity of $\mathcal{N}_3$ means that w' is not only a function of q' but also of $\overline{q}$. Thus this method gives the vertical motion attributed to q' *appropriate to that particular distribution of* $\overline{q}$. This property is perhaps in accord with what one might expect but note that it implies that this is not an invariant way to attribute vertical motion to a given potential vorticity anomaly; i.e. the results depend on the properties of the surrounding atmosphere.

Significant insight into attribution comes from noting that the elliptic equations defining both the potential vorticity and the vertical motion suggest an electrostatic analogy. Bishop and Thorpe (1994) and Thorpe and Bishop (1995) note that potential vorticity can be regarded as a source for the geostrophic streamfunction much as the electric charge is a source for the electric potential. In addition the static stability of the surrounding, or background, atmosphere can be characterised as analogous to the dielectric constant. The streamfunction attributed to the potential vorticity source will be different depending on the properties of the surrounding atmosphere. Also Clough et al 1996 point out that the omega equation can be similarly interpreted where $\nabla.\underline{Q}$ is the source of vertical motion. In both cases the static stability determines this dielectric constant, however for the omega equation it has a slightly different dependence on static stability due to the difference between $\mathcal{N}_1$ and $\mathcal{N}_2$.

It is worth remembering that it is also possible, and attractive, to attribute mechanisms as well as geographically defined anomalies. For example it is possible to divide the omega equation forcing term S into parts due to vorticity advection and thermal advection or alternatively into isentropic upgliding, boundary thermal advection and potential vorticity advection; see Hoskins, McIntyre and Robertson (1985). Note however that the vertical motion attributed to each of the mechanisms must partially cancel each other. This is because $\nabla.\underline{Q}$ is a frame-independent form whereas each of the partitioned elements are frame-dependent. Also a combination of these two forms of attribution is possible whereby local anomalies of a specific forcing term are identified and the vertical motion attributable to them found.

The alternative method to calculate w' from equation (9) might seem to give a way to attribute vertical motion to a potential vorticity anomaly in an unambiguous way. But note that $\mathcal{N}_1$ and $\mathcal{N}_2$ require the horizontal average static stability in the domain of interest. This is determined by the background potential vorticity distribution. So even this way to find w' is not invariant in the sense described here. Also in this method the vertical motion attributable to the background potential vorticity is not only a function of $\overline{q}$ but also a function of q'. To see this subtract equation (9) from equation (7):

$$\overline{w} = \mathcal{N}_2^{-1}\left[\mathcal{N}_3\left[\mathcal{N}_1^{-1}\left[q\right]\right]\right] - \mathcal{N}_2^{-1}\left[\mathcal{N}_3\left[\mathcal{N}_1^{-1}\left[q'\right]\right]\right] \qquad (10)$$

This property, namely that the background vertical motion is a function of the potential vorticity of both the background state and the anomaly, is not easy to interpret physically. It leads us to suggest that the use of equation (8) is simpler to interpret.

In summary it is attractive to attempt to attribute vertical motion as well as geostrophic flow and temperature to particular potential vorticity anomalies. This makes explicit the fact that most of the ageostrophic motion can be calculated from the geostrophic state for which the potential vorticity is the so-called "slaving" variable. (The

part of the ageostrophic motion that cannot be so described is the genuinely unbalanced motion due to inertia-gravity waves etc.) These anomalies might be clearly associated with a given weather system and they are the fundamental building blocks of atmospheric dynamics due to the potential vorticity conservation principle. Whilst hopefully illuminating, this general description of the possibilities of attribution is abstract so that it is appropriate that we now use the framework to consider an important specific problem in the mesoscale meteorology of extra-tropical cyclones. The goal is to solve the problem of whether, and how much, vertical motion can be attributed to the tropopause fold structure present in many extra-tropical cyclones.

3. Tropopause fold problem

Extreme undulations of the tropopause, sometimes involving tropopause folds, are commonplace in mature extratropical cyclones. In some cases it is tempting to attribute the onset of certain mesoscale phenomena, such as convection and vortices, to the descent of the tropopause to levels near the boundary layer; see observational evidence from Browning and Golding (1995) and Browning and Reynolds (1994). It is also clear that these tropopause folds are important in cross-tropopause transport and probably in the dynamics of the cyclone itself; see Hirschberg and Fritsch (1991). In this paper the association between mesoscale features in the pattern of vertical motion and the presence of a tropopause fold is examined. The term "fold" will be used here to mean a tropopause undulation however extreme.

To simplify the dynamical problem we will consider a two-dimensional frontal zone which exhibits both a surface and an upper-level front. The zone will be subject to frontogenesis and so a characteristic vertical motion pattern will exist. Solutions have been obtained by solving numerically the Sawyer-Eliassen cross-frontal circulation equation. The semi-geostrophic (SG) theory in two dimensions is used as the basic tool for the analysis. This theory has a very similar equation structure to the quasi-geostrophic set but it is more accurate. In particular for deductions of vertical motion, at a given time, the theory is rather accurate in this case. For the derivation of simple building blocks the SG system is superior to other approximate sets as it exhibits a simple form of omega equation.

Stretching and shearing deformation frontogenesis have rather distinctive patterns of vertical motion attributable to the fold. A key factor is that the fold is usually a mesoscale feature embedded in a larger-scale pattern of forcing. The relative positions of the fold and this forcing, the magnitude of the potential vorticity anomaly in the fold, and the horizontal extent of the fold together determine the mesoscale features of vertical motion attributable to the fold. Imposing stretching and/or shearing deformation implies that on a larger scale, not considered explicitly in these calculations, there are potential vorticity distributions to which the deformation is attributable. In effect there are three horizontal scales: that of the potential vorticity distribution leading to the deformation, that of the potential vorticity distribution associated with a gently-sloping tropopause, and that of the mesoscale tropopause fold potential vorticity anomaly. The particular horizontal scales involved will become clearer in the calculations to be presented later.

Another consequence of the tropopause fold is that there is reduced static stability below the large potential vorticity contained in the fold. It is therefore important in considering, for example, the triggering of convection to ascertain whether there is a favourable co-location of the reduction in static stability due to the tropopause fold and the changes in the vertical motion pattern. Convective activity can be triggered by a lowered tropopause if this can occur. Additionally differential humidity advection caused

by the fold may also have an important role in triggering convection. The latter is not considered in this paper.

4. Resumé of Semi-geostrophic equations

Here we summarize the two-dimensional semi-geostrophic potential vorticity inversion and omega equations. The theory consists of an approximate equation set which is more accurate than the quasi-geostrophic set. The equations can, in addition, be transformed to geostrophic momentum coordinates and are described in Hoskins (1975) and in Hoskins and Draghici (1977). The transformation to geostrophic momentum (GM) coordinates is given by: $X = x + v_g/f$ and $Z = z$.

In two dimensions the definition of the semi-geostrophic potential vorticity in terms of the modified geopotential is:

$$P = \frac{\frac{\partial^2 \Phi}{\partial Z^2}}{f^2 - \frac{\partial^2 \Phi}{\partial X^2}} \tag{11}$$

where P is the non-dimensional potential vorticity given by the expression: $P = (\frac{g}{f^3 \theta_0}) \underline{\zeta} . \nabla \theta$, $\underline{\zeta}$ is the geostrophic vorticity, ϕ is the geopotential and $\Phi = \phi + \frac{1}{2}({u_g}^2 + {v_g}^2)$ is the modified geopotential.

The Sawyer-Eliassen cross-frontal circulation equation in these coordinates is:

$$\frac{\partial}{\partial X}\left(P\frac{\partial \Psi}{\partial X}\right) + \frac{\partial^2 \Psi}{\partial Z^2} = \frac{2Q}{f^2} \tag{12}$$

where $u = -\partial\Psi/\partial Z$ and $w = \frac{\zeta}{f} w^*$ and $w^* = \partial\Psi/\partial X$ are the ageostrophic wind components, Ψ is the ageostrophic flow streamfunction, and Q is the geostrophic forcing given in the transformed coordinates by:

$$Q = f\left(-\frac{\partial u_g}{\partial X}\frac{\partial v_g}{\partial Z} + \frac{\partial v_g}{\partial X}\frac{\partial u_g}{\partial Z}\right) \tag{13}$$

The omega equation for the vertical motion is obtained by simple horizontal differentiation of equation (12). It is worth commenting on the form of these equations as it has been noted that they are similar to the quasi-geostrophic equations except that they refer to the GM space. Equation (11) shows that, in GM space, the potential vorticity is not given by a simple Laplacian. However Thorpe and Bishop (1995) show that in geometric coordinates the semi-geostrophic potential vorticity is interpretable in terms of an electrostatic analogy with potential vorticity as the source of the balanced flow and temperature. Eliassen (1962) discusses the fact that equation (12) is consistent with an electrostatic analogy, with Q being the source of the ageostrophic motion. In the cross-frontal circulation equation it is the potential vorticity which acts as the dielectric constant for semi-geostrophic theory in GM coordinates whereas the static stability plays this role for the quasi-geostrophic case (see equation(4)).

5. Attribution results for the tropopause fold

(a) *General aspects*

It is clear from examination of the SG equations that a tropopause fold is related to the vertical motion pattern in two distinct ways. The first is, of course, the Q forcing. This is in part determined by the existence of the potential vorticity anomaly contained in the fold as well as by the background potential vorticity, including that implied by the surface thermal pattern. The second is the role of the potential vorticity as a dielectric factor as it is a coefficient in the Sawyer-Eliassen equation. This equation is the counterpart of the two-dimensional quasi-geostrophic omega equation where the coefficient is the static stability. Here we will set-up some simple idealised problems which isolate these two effects. It is shown here that the combination of these two effects allows the attribution of a pattern of vertical motion to the tropopause fold which includes, in different regions, a decrease and an increase in vertical motion. The goal is to quantify the effect on the vertical motion pattern and static stability due to a tropopause fold. This will be done at an instant in time. The time evolution is postponed to later studies along these lines.

Some previous studies are relevant to the role of potential vorticity as analogous to a "dielectric" factor. Eliassen (1962) derived the Green's function solution for the ageostrophic circulation. Thorpe and Emanuel (1985) studied the role of potential vorticity in the Sawyer-Eliassen equation for situations where the potential vorticity is modified locally due to latent heat release. Chan and Cho (1989) examined the effect of mesoscale potential vorticity anomalies in stimulating rainbands at fronts. Moore (1993) considered the tropopause descent for idealised two-dimensional semi-geostrophic frontogenesis.

To gain some insight into the vertical motion attributable to the fold it is first convenient to manipulate the SG Sawyer-Eliassen equation. The streamfunction Ψ can be divided into a part, $\overline{\Psi}$, which is the solution of the equation using the background potential vorticity everywhere and a (not necessarily small) deviation from that, Ψ', due to the presence of the tropopause fold potential vorticity anomaly. So the equation for Ψ' is obtained by subtracting the equation for $\overline{\Psi}$ from the full equation (12) to give:

$$\frac{\partial}{\partial X}\left(P\frac{\partial \Psi'}{\partial X}\right)+\frac{\partial^2 \Psi'}{\partial Z^2}=-\frac{\partial}{\partial X}\left(P'\overline{w}^*\right)+\frac{2Q'}{f^2} \tag{14}$$

where Q' is the incremental Q attributable to the fold potential vorticity anomaly.

Consider the two forcing terms on the right-hand-side. The first term will be referred to as the "ageostrophic" forcing as it depends on the background vertical motion as well as the fold potential vorticity anomaly whilst the second term will be referred to as the additional "geostrophic" forcing as it depends on the geostrophic flow and temperature due to the fold potential vorticity anomaly.

1. *Ageostrophic forcing*: shows that in regions of background ascent (descent) the edge of the fold on the warm air side represents a positive (negative) forcing of the streamfunction and the edge on the cold air side has the opposite sign of forcing. It arises from that part of the dielectric factor acting due to the fold potential vorticity anomaly. This form of the circulation equation allows one to provide a simple rule-of-thumb for this ageostrophic contribution to the vertical motion attributable to the potential vorticity anomaly of the fold:

   - in the fold itself it is of the opposite sign to that of the background vertical motion, whilst
   - adjacent to the fold, in the tropospheric air, it is of the same sign as the background vertical motion.

   The sense of the vertical motion, attributable to the fold, in the adjacent tropospheric air is a little unexpected but potentially of significance if the mesoscale detail in the

vertical motion pattern is to be related to subsequent weather development. In essence the fold acts to weaken the background vertical motion within the fold but amplify it in the adjacent tropospheric air. The mathematical form of this term shows that the size of this effect will depend on how large the horizontal gradient of potential vorticity is across the tropopause fold.

2. *Geostrophic forcing*: contribution is an implicit function of the potential vorticity distribution. The non-linear dependence of potential vorticity on the pressure field means that Q' depends on the background as well as on the fold potential vorticity. It is the aim of this paper to attempt to elucidate the nature of this functional dependence to provide some simpler building blocks for attribution. We postpone detailed discussion of this factor until the numerical solutions of the Sawyer-Eliassen equation are presented in the next section.

(*b*) *Realistic tropopause structure*

In this section the vertical motion attributable to the tropopause fold will be calculated using both the geostrophic and ageostrophic contributions noted in the previous section. Realistic, but idealised, tropopause structures will be used as the problem will be solved numerically for several archetypical cases using the two-dimensional SG model. (Note that all solutions are shown in physical space.) The geostrophic flow is a consequence of the imposed boundary thermal pattern, which is kept fixed for the sake of clarity, and the internal potential vorticity structure which will be varied. Solutions of the omega equation will be presented in which deformation and/or shear is imposed. It should be stressed that these structures are assumed and have not arisen from a time integration from simpler initial conditions. Consequently the vertical motion will imply an evolution of the assumed folded potential vorticity pattern. No attempt is made here to calculate that evolution.

The potential vorticity pattern to be assumed is such that the thermal gradient along the tropopause is imposed but the physical location of the tropopause fold is part of the solution. Furthermore we impose the condition that the isentrope which just grazes the tropopause on the cold air side descends to graze the surface on the warm air side on the ground. This is not an uncommon situation for observed fronts but it is also used here to keep the same boundary conditions for all cases. Typically we will compare solutions for a deep tropopause fold and a shallow tropopause fold. The shallow fold case will also be referred to as the background state, as described in the previous section. The difference between these two states represents the potential vorticity anomaly of the fold to which we wish to attribute a unique vertical motion pattern. Therefore we are now going to use the method of attribution implied by equation (8). (Note that therefore we are not going to solve equation (14) directly.)

In Figure 1 the geostrophic flow and temperature distribution is given for the deep fold and the shallow fold. (For all the figures the horizontal domain is $2000km$ and the vertical domain is $10km$. The potential vorticity is constant in the troposphere ($0.3PVU$) and it jumps to another constant value in the stratosphere ($1.5PVU$). The calculations have been performed with a horizontal resolution of $40km$ and a vertical resolution of $50m$.) The calculations show that there is a small reduction in static stability directly beneath the tropopause fold in the troposphere. This is in accord with simple potential vorticity inversion concepts.

To assess the relative magnitudes of the roles of the "ageostrophic" forcing due to the anomaly in potential vorticity and the "geostrophic" forcing caused by the change in Q due to the anomaly, we will also calculate the vertical motion for the deep fold using the

appropriate potential vorticity distribution, but using the Q pattern for the shallow fold. (In terms of equation (14) this is equivalent to retaining only the ageostrophic forcing.)

(i) *Stretching deformation*

In this case we take $\partial u_g/\partial X = -\alpha$ in equation (13) as a constant (with $\alpha = 1 \times 10^{-5} s^{-1}$) and $\partial u_g/\partial Z = 0$. This corresponds to deformation-forced frontogenesis and the commonly-used value of stretching deformation has been assumed for this study.

For the shallow fold the Q pattern consists of a positive region in the baroclinic zone but with a local maxima in the fold and at the ground; see Figure 2(a). The vertical motion associated with the shallow fold is a simple thermally-direct circulation; see Figure 2(b). The vertical motion is weak as to be expected for the chosen value of the deformation rate. The vertical motion and Q pattern associated with the deep fold has a rather similar structure to that of the shallow fold case but with a local maximum in ascent on the warm air side of the fold tip; see Figure 3. This is a consequence of the choice of potential vorticity distribution which dictates the relative location of the fold and the dilatation axis of the deformation flow.

In assessing the vertical motion attributable to the deep fold potential vorticity anomaly we expect there to be two contributions: from the ageostrophic and additional geostrophic forcings:

1. *Ageostrophic forcing*: To assess the role of the ageostrophic forcing we must look at the background vertical motion from the shallow fold case in the vicinity of the deep fold anomaly. From Figure 2(b) it can be seen that the deep fold lies in a region of background ascent. Therefore we expect the deep fold anomaly to reduce the ascent in the anomaly itself but increase the ascent in the warm air ahead of the fold.
2. *Geostrophic forcing*: The other contribution to the vertical motion attribution comes from the influence of the deep fold potential vorticity anomaly on Q. To see this we calculate the Q difference field (Q' =deep - shallow). From equation (13) it can seen that $Q' = f\alpha\partial v_g'/\partial Z$, where v_g' is the additional along-front flow due to the fold potential vorticity anomaly. The vertical shear, along the sloping frontal surface, attributable to the fold is in fact predominantly positive although this is difficult to deduce a priori without numerical calculation. In Figure 4(a) it can be seen that Q' has a positive zone associated with the potential vorticity anomaly with local minima above and below the anomaly. From equation (12) the vertical motion is approximately proportional to $-\partial Q'/\partial X$ and so this distribution of Q' will force ascent ahead and descent behind the fold.

It appears that in this case the two effects will reinforce each other. The vertical motion difference, which can be attributed to the potential vorticity anomaly of the deep fold, can be obtained following equation (8), by taking the difference of the vertical motion in the deep fold case and that in the shallow fold case (i.e. deep-shallow). It has a clear dipole distribution with ascent ahead and descent within and behind the anomaly (peak value of about $0.5 cms^{-1}$); see Figure 4(b). Increased ascent in the warm, already ascending, air can therefore be attributed to the potential vorticity anomaly of the fold. This can be further seen as the vertical motion of the deep fold case is well predicted by taking the shallow fold Q forcing but for the deep fold potential vorticity distribution (not shown).

The zone of reduced static stability due to the deep fold potential vorticity anomaly resides in a zone of ascent thus suggesting the possibility of the triggering of convection in this case.

(ii) *Shearing deformation*

In this case we take $\partial u_g/\partial X = 0$ and $\partial u_g/\partial Z = s$ a constant. A value of $s = 5 \times 10^{-3} s^{-1}$ is used to illustrate the case of shearing deformation. This is a moderate shear for a cyclonic storm-track flow.

The shallow fold Q forcing has more structure than for the case of deformation forcing. The surface front has a dipole in Q positively correlated with the temperature pattern whilst the upper front has the reverse orientation for this dipole. The link between the upper front and surface front dipoles is such that there is negative Q in mid-troposphere; see Figure 5(a). There is now descent over the surface front with ascent ahead of the upper front/potential vorticity-fold structure; see Figure 5(b).

For the deep fold the Q field now has a sloping zone of positive values in the frontal zone stretching from the ground into the tropopause fold; see figure 6(a). This forcing leads to a vertical motion field which has a substantially different structure to that for the shallow fold; see Figure 6(b). It has a classical thermally-direct circulation but with larger magnitude and smaller cross-frontal scale than the stretching deformation case. The tropopause fold now lies almost exactly along the interface between the ascent and descent regions with perhaps a small bias to ascent.

Consider the two contributions to w':

1. *Ageostrophic forcing*: In the vicinity of the deep fold anomaly there is background descent, as can be seen in Figure 5(b). Therefore the ageostrophic term would imply descent ahead of the fold and ascent within the fold, i.e. a thermally-indirect circulation.
2. *Geostrophic forcing*: From equation (13) it can seen that $Q' = fs\partial v_g'/\partial X$, where v_g' is the additional along-front flow due to the fold potential vorticity anomaly. The horizontal shear, perpendicular to the sloping frontal surface, attributable to the fold is positive as might be expected from simple inversion of an isolated positive potential vorticity anomaly. In Figure 7(a) the Q' field is dominated by the positive values in the potential vorticity anomaly and it is surprisingly similar to that for the case of stretching deformation. Hence from the geostrophic contribution we expect there to be ascent forced ahead of the fold and descent within the fold.

Thus in this case the ageostrophic and geostrophic contributions oppose one another. Obtaining the vertical motion pattern, attributable to the potential vorticity anomaly, from the numerical solutions, there is a simple dipole oriented with ascent to the warm side of the potential vorticity anomaly (peak values of around $4cms^{-1}$); see Figure 7(b). Thus the geostrophic contribution to the forcing is dominant. The prediction of the deep fold vertical motion using the shallow fold Q (not shown) is poorer in this case which shows that the dominant effect of the potential vorticity anomaly is the change to the Q-vector forcing. The zone of reduced static stability due to the potential vorticity anomaly is mostly in the zone of descent.

(iii) *Combined shear and deformation*

It is known from Shapiro (1981) that the combination of cold advection (negative shearing deformation) and confluence is conducive to the descent of the tropopause fold. For this case we take values of $\alpha = 1.0 \times 10^{-5} s^{-1}$ for the confluence and $s = -2.0 \times 10^{-3} s^{-1}$ for the shear component. (It should be noted that unless these values vary in time in the way prescribed by Keyser and Pecnick (1985) then the front will not remain two-dimensional.)

The shallow fold has a pattern of Q with positive values along the frontal zone; see Figure 8(a). The pattern of Q is similar to that for shear deformation alone, given

in Figure 5(a), but with the opposite sign. Therefore for the chosen values of α and s the shear contribution appears to be dominant. The vertical motion pattern has strong descent in the upper front, as anticipated by Shapiro, with ascent in the warm air; see Figure 8(b). Notice that the vertical motion is reversed compared to the case with shear alone because now $s < 0$.For the deep fold case the Q pattern is even more complex now with the surface front having a dipole of opposite sign to the case with shear alone; see Figure 9(a). The fold is characterised by essentially positive values of Q. This leads to a pattern of descent in the fold itself with significant ascent in the surface frontal zone and in the warm air ahead of the front; see Figure 9(b).

The two forcing terms for the vertical motion attributable to the fold are:

1. *Ageostrophic forcing*: In the vicinity of the deep fold anomaly there is background ascent, as can be seen in Figure 8(b). Therefore the ageostrophic term would imply ascent ahead of the fold and descent within the fold, i.e. a thermally-direct circulation.
2. *Geostrophic forcing*: In this case Q' has contributions from both the vertical and horizontal shears of the additional along-front wind attributable to the fold. Numerical calculation shows that the Q' pattern is now reversed compared to the previous cases with negative values in the region of the potential vorticity anomaly; see Figure 10(a). This is due to the dominance of the $fs\partial v'_g/\partial X$ term in Q', noting that now $s < 0$. Therefore we expect the additional Q forcing to contribute a thermally-indirect component to the vertical velocity field.

Again in this case the two forcing contribution oppose each other. The numerical solution for the vertical motion attributable to the fold potential vorticity anomaly consists of a thermally indirect dipole with values in excess of $1.5cms^{-1}$; see Figure 10(b). Therefore the geostrophic forcing of the vertical motion attributable to the fold is the dominant contribution in this case. The predicted field ignoring the effect of the potential vorticity anomaly on the Q-vector forcing is therefore not a very accurate portrayal of the pattern with the deep fold (not shown).

In this case the region of reduced static stability is optimally placed with respect to the increased ascent attributable to the potential vorticity anomaly of the deep fold suggesting a strong potential for triggering of convection.

6. Conclusions

It has been shown that there are two contributions to the forcing of vertical motion attributable to a tropopause fold potential vorticity anomaly. These are called the ageostrophic and geostrophic contributions. At least for the cases considered here it would appear that the geostrophic contribution is the largest, although this cannot be regarded as a general result. For two-dimensional cases the additional geostrophic forcing of vertical motion due to the fold is a linear function of the along-front flow. This in turn is a more complicated implicit function of the fold potential vorticity distribution. However from the numerical results it would appear that a good approximate rule is that $Q' \propto def \times P'$ where def is the dominant part of the imposed deformation rate, i.e. either confluence or shearing deformation. Therefore the vertical motion attributable to the fold is crudely given by: $w' \propto -def \times \partial P'/\partial X$, which is the potential vorticity advection component of the forcing. It should be stressed that these relationships do not have a general validity and in particular it is as yet unclear what might happen for three-dimensional fold structures. The size of the ageostrophic contribution to the forcing of the vertical motion attributable to the fold depends strongly on how large the gradient of potential vorticity

is across the fold. If the ageostrophic contribution were to be larger then the simple approximations just mentioned would be modified.

For the cases considered here the contribution to the vertical motion attributable to the fold from the so-called geostrophic forcing is dominant but it is significantly modulated by the ageostrophic forcing. In these circumstances the vertical motion attributable to the fold is mostly due to differential potential vorticity advection. Hence, if there is frontogenesis, there is ascent in the warm tropospheric air ahead of the fold and descent behind the fold which can be uniquely attributed to the fold potential vorticity anomaly.

It has been shown that the tropopause fold feature typical of extratropical cyclones is not passive but responsible for producing a significant degree of mesoscale detail in the vertical motion and static stability distributions. These may or may not be responsible for generating mesoscale weather phenomena, such as convection or vortices, but these studies are suggestive that such is at least a possibility. It is important to extend these ideas to three-dimensions as tropopause folds are usually highly three dimensional.

This mesoscale problem has provided an example of how attribution ideas can be posed to give insight into the dynamics of the atmosphere. It is clear that the success of attribution relies on the existence of a simple set of building blocks with which to describe the dynamics. Semi-geostrophic theory is a good example of such a set.

Figure Captions

Figure 1: (a) Section showing the potential temperature (contour interval 5K), flow along the front (contour interval $5ms^{-1}$) and potential vorticity (bold contour indicates the location of the tropopause) for the deep fold case, (b) Same for the shallow fold.

Figure 2: (a) Q for deformation frontogenesis for the shallow fold (contour interval $4.0 \times 10^{-12}s^{-3}$ with dashed contours negative) and (b) Vertical velocity for the same case (contour interval $0.2cms^{-1}$ with a maximum value of $0.87cms^{-1}$).

Figure 3: (a) Q for deformation frontogenesis for the deep fold and (b) Vertical velocity for the same case. (Contour intervals as in figure 2 but maximum vertical velocity is now $1.1cms^{-1}$.)

Figure 4: (a) The difference in Q between the deep and shallow folds, which is attributable to the fold potential vorticity anomaly, for deformation frontogenesis (contour interval $2 \times 10^{-12}s^{-3}$) and (b) Vertical velocity difference for the same case (contour interval $0.1cms^{-1}$ with a maximum value of $0.29cms^{-1}$).

Figure 5: (a) Q for shear frontogenesis for the shallow fold (contour interval $8 \times 10^{-12}s^{-3}$ and (b) Vertical velocity for the same case (contour interval $1cms^{-1}$ with a maximum of $4.4cms^{-1}$).

Figure 6: (a) Q for shear frontogenesis for the deep fold (contour interval $8 \times 10^{-12}s^{-3}$) and (b) Vertical velocity for the same case (contour interval $1cms^{-1}$ with a maximum of $2.7cms^{-1}$).

Figure 7: (a) The difference in Q between the deep and shallow folds, which is attributable to the fold potential vorticity anomaly, for shear frontogenesis (contour interval $8 \times 10^{-12}s^{-3}$ and (b) Vertical velocity difference for the same case (contour interval $1cms^{-1}$ with a maximum value of $3.9cms^{-1}$).

Figure 8: (a) Q for combined deformation and shear frontogenesis for the shallow fold (contour interval $8 \times 10^{-12}s^{-3}$) and (b) Vertical velocity for the same case (contour

interval $0.4cms^{-1}$ with a maximum of $1.5cms^{-1}$).

Figure 9: (a) Q for combined deformation and shear frontogenesis for the deep fold (contour interval $8 \times 10^{-12}s^{-3}$) and (b) Vertical velocity for the same case (contour interval $0.4cms^{-1}$ with a maximum of $1.6cms^{-1}$).

Figure 10: (a) The difference in Q between the deep and shallow folds, which is attributable to the fold potential vorticity anomaly, for combined deformation and shear frontogenesis (contour interval $0.4 \times 10^{-12}s^{-3}$ and (b) Vertical velocity difference for the same case (contour interval $0.4cms^{-1}$ with a maximum value of $1.5cms^{-1}$).

APPENDIX

The definition of the terms in the QG model are:

geostrophic derivative:

$$D_g = \frac{\partial}{\partial t} + \underline{v}_g.\nabla \tag{A.1}$$

geostrophic streamfunction:

$$\psi = \frac{p'}{\rho_0 f_0} \tag{A.2}$$

buoyancy and hydrostatic relation:

$$b' = \frac{g}{\theta_0}\theta' = f_0\frac{\partial \psi}{\partial z} \tag{A.3}$$

QG potential vorticity:

$$q = f + \xi_g + \frac{\partial}{\partial z}\left(\frac{f_0}{N^2}b'\right) \tag{A.4}$$

geostrophic wind:

$$(u_g, v_g) = \left(-\frac{\partial \psi}{\partial y}, \frac{\partial \psi}{\partial x}\right) \tag{A.5}$$

relative vorticity:

$$\xi_g = \frac{\partial v_g}{\partial x} - \frac{\partial u_g}{\partial y} = \nabla_h{}^2\psi \tag{A.6}$$

Q-vector:

$$\underline{Q} = \left(-\frac{\partial u_g}{\partial x}\frac{\partial b'}{\partial x} - \frac{\partial v_g}{\partial x}\frac{\partial b'}{\partial y}, -\frac{\partial u_g}{\partial y}\frac{\partial b'}{\partial x} - \frac{\partial v_g}{\partial y}\frac{\partial b'}{\partial y}\right) \tag{A.7}$$

differential operators:

$$\mathcal{N}_1 = \nabla_h{}^2 + \frac{\partial}{\partial z}\left(\frac{f_0{}^2}{N^2}\frac{\partial}{\partial z}\right) \tag{A.8}$$

$$\mathcal{N}_2 = N^2\nabla_h{}^2 + f_0{}^2\frac{\partial^2}{\partial z^2} \tag{A.9}$$

$$\begin{aligned}\mathcal{N}_3[\psi] = {} & 2f_0\left(\frac{\partial^2\psi}{\partial x\partial z}\nabla_h{}^2\frac{\partial \psi}{\partial y} - \frac{\partial^2\psi}{\partial y\partial z}\nabla_h{}^2\frac{\partial \psi}{\partial x}\right) \\ & +2f_0\left(\frac{\partial^2\psi}{\partial x\partial y}\frac{\partial}{\partial z}\left(\frac{\partial^2\psi}{\partial x^2} - \frac{\partial^2\psi}{\partial y^2}\right) - \frac{\partial^3\psi}{\partial x\partial y\partial z}\left(\frac{\partial^2\psi}{\partial x^2} - \frac{\partial^2\psi}{\partial y^2}\right)\right)\end{aligned} \tag{A.10}$$

Other quantities are as follows: p' is the deviation pressure from a hydrostatic reference state, ρ_0 is the constant density, f_0 is a constant value of the Coriolis parameter, and N^2 is the square of the Brunt-Vaisala frequency taken to be a function of height only.

Acknowledgements

Grateful thanks are extended to NCAR, and in particular to Bob Gall and Rich Rotunno, for supporting the author's summer visit to NCAR during which time this research was begun. Helpful discussions with Bill Blumen and Keith Browning concerning tropopause fold dynamics took place at NCAR and at Reading. Thanks go to Sid Clough and Craig Bishop for many useful discussions on attribution. Comments from George Craig and Doug Parker improved the clarity of the exposition.

References

Birkett, H. R. and Thorpe, A. J.	1997	Superposing semi-geostrophic potential vorticity anomalies. *Q. J. R. Meteorol. Soc.*, **123**, in press
Bishop, C. H. and Thorpe, A. J.	1994	Potential vorticity and the electrostatics analogy: quasi-geostrophic theory. *Q. J. R. Meteorol. Soc.*, **120**, 713-731
Browning, K. A. and Golding, B. W.	1995	Mesoscale aspects of a dry intrusion within a vigorous cyclone. *Q. J. R. Meteorol. Soc.*, **121**, 463-493
Browning, K. A. and Reynolds, R.	1994	Diagnostic study of a narrow cold frontal rainband and severe winds associated with a stratospheric intrusion. *Q. J. R. Meteorol. Soc.*, **120**, 235-257
Chan, D. S. T. and Chou, H-R.	1989	Meso-beta scale potential vorticity anomalies and rainbands. Part I: Adiabatic dynamics of potential vorticity anomalies. *J. Atmos. Sci.*, **46**, 1713-1723
Clough, S. A., Davitt, C. S. A. and Thorpe, A. J.	1996	Attribution concepts applied to the omega equation. *Q. J. R. Meteorol. Soc.*, **122**, 1943-1962
Davis, C. A. and Emanuel, K. A.	1991	Potential vorticity diagnostics of cyclogenesis. *Mon. Wea. Rev.*, **119**, 1929-1953
Davis, C. A.	1992	Piecewise potential inversion. *J. Atmos. Sci.*, **49**, 1397-1411
Eliassen, A.	1962	On the vertical circulation in frontal zones. *Geophys. Publikasjoner*, **24**, No. 4, 147-160
Hirschberg, P. A. and Fritsch, M. J.	1991	Tropopause undulations and the development of extratropical cyclones. Part II Diagnostic analysis and conceptual model. *Mon. Wea. Rev.*, **119**, 518-550
Hoskins, B. J.	1975	The geostrophic momentum approximation and the semi-geostrophic equations. *J. Atmos. Sci.*, **32**, 233-242
Hoskins, B. J. and Draghici, I.	1977	The forcing of ageostrophic motion according to the semi-geostrophic equations and in an isentropic model. *J. Atmos. Sci.*, **34**, 1858-1867
Hoskins, B. J., McIntyre, M. E. and Robertson, A. W.	1985	On the use and significance of isentropic potential vorticity maps *Q. J. R. Meteorol. Soc.*, **111**, 877-946
Keyser, D. and Pecknick, M. J.	1985	A two-dimensional primitive equation model of frontogenesis forced by confluence and horizontal shear. *J. Atmos. Sci.*, **42**, 1259-1282
Moore, G. W. K.	1993	The development of tropopause folds in two-dimensional models of frontogenesis. *J. Atmos. Sci.*, **50**, 2321-2334
Shapiro, M. A.	1981	Frontogenesis and geostrophically forced secondary circulations in the vicinity of jet stream-frontal zone systems. *J. Atmos. Sci.*, **38**, 954-973
Stein, U. and Alpert, P.	1993	Factor separation in numerical simulations. *J. Atmos. Sci.*, **50**, 2107-2115

Thorpe, A. J. and Emanuel, K. A. 1985 Frontogenesis in the presence of small stability to slantwise convection. *J. Atmos. Sci.*, **42**, 1809-1824

Thorpe, A. J. and Bishop, C. H. 1995 Potential vorticity and the electrostatics analogy: Ertel-Rossby formulation. *Q. J. R. Meteorol. Soc.*, **121**, 1477-1495

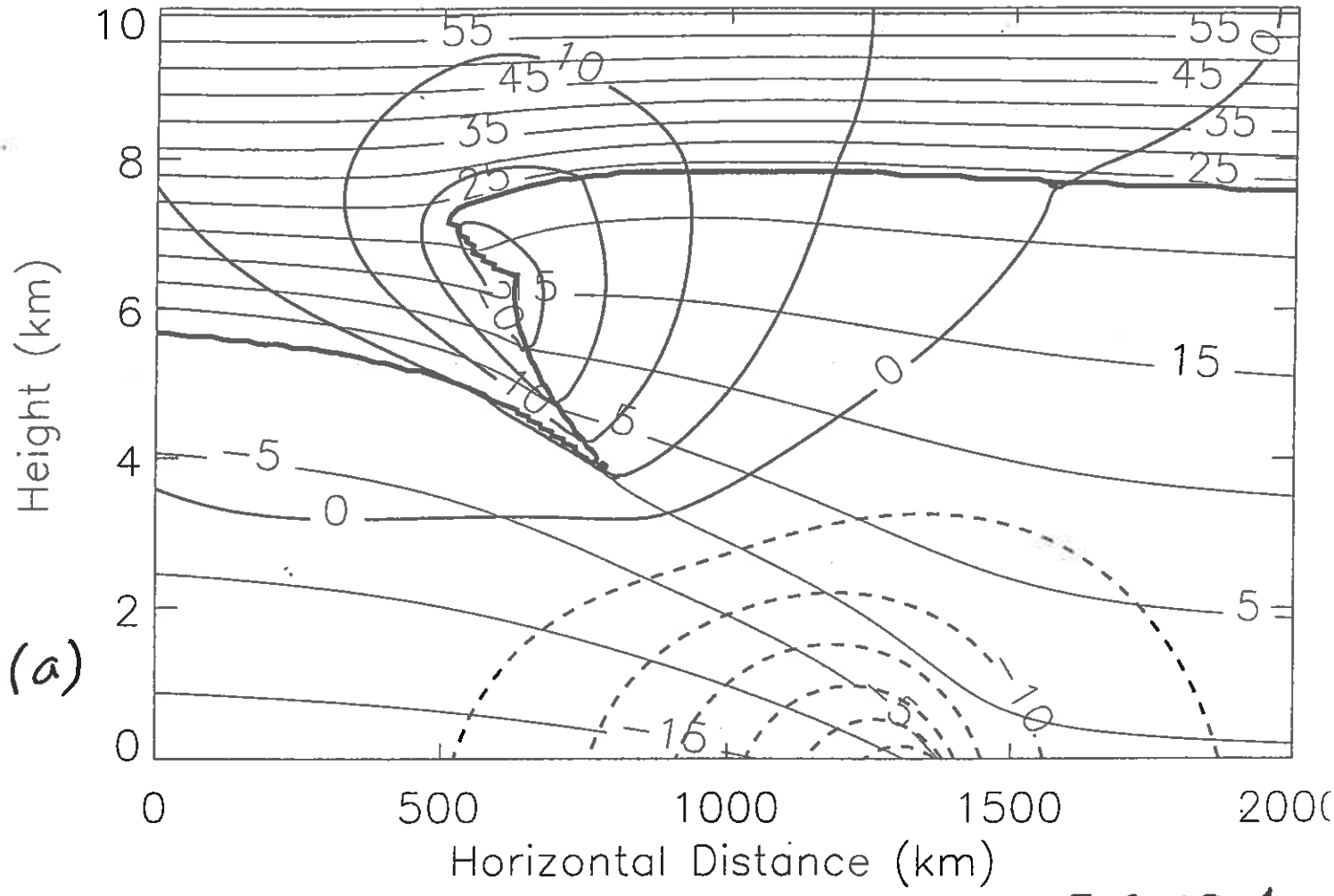
(a)
Height (km)
Horizontal Distance (km)
0
500
1000
1500
2000
0
2
4
6
8
10
55
45
35
25
15
10
5
0
-5
-10
-15

FIGURE 1

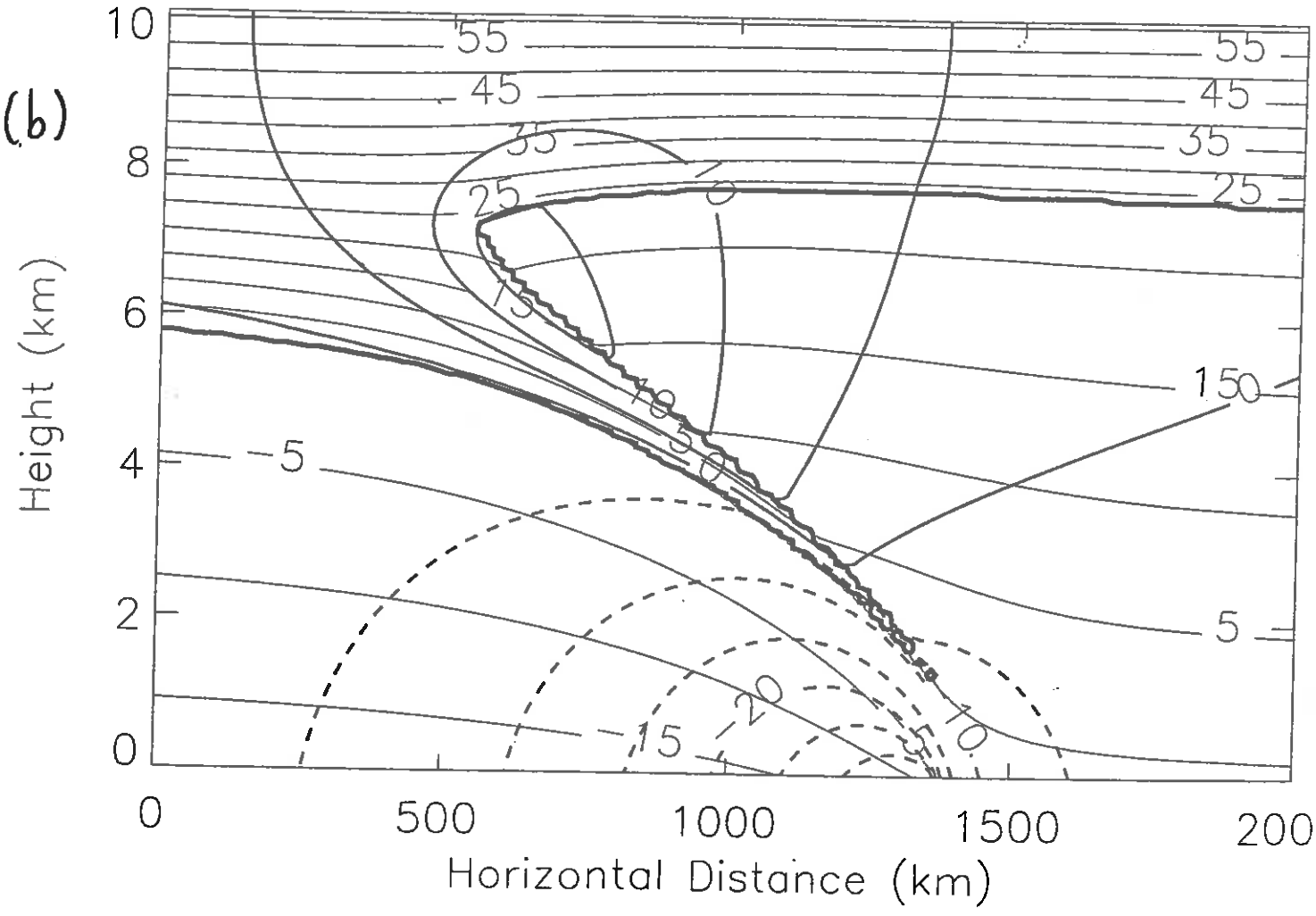
(b)
Height (km)
Horizontal Distance (km)
0
500
1000
1500
200
0
2
4
6
8
10
55
45
35
25
15
10
5
0
-5
-10
-15
150

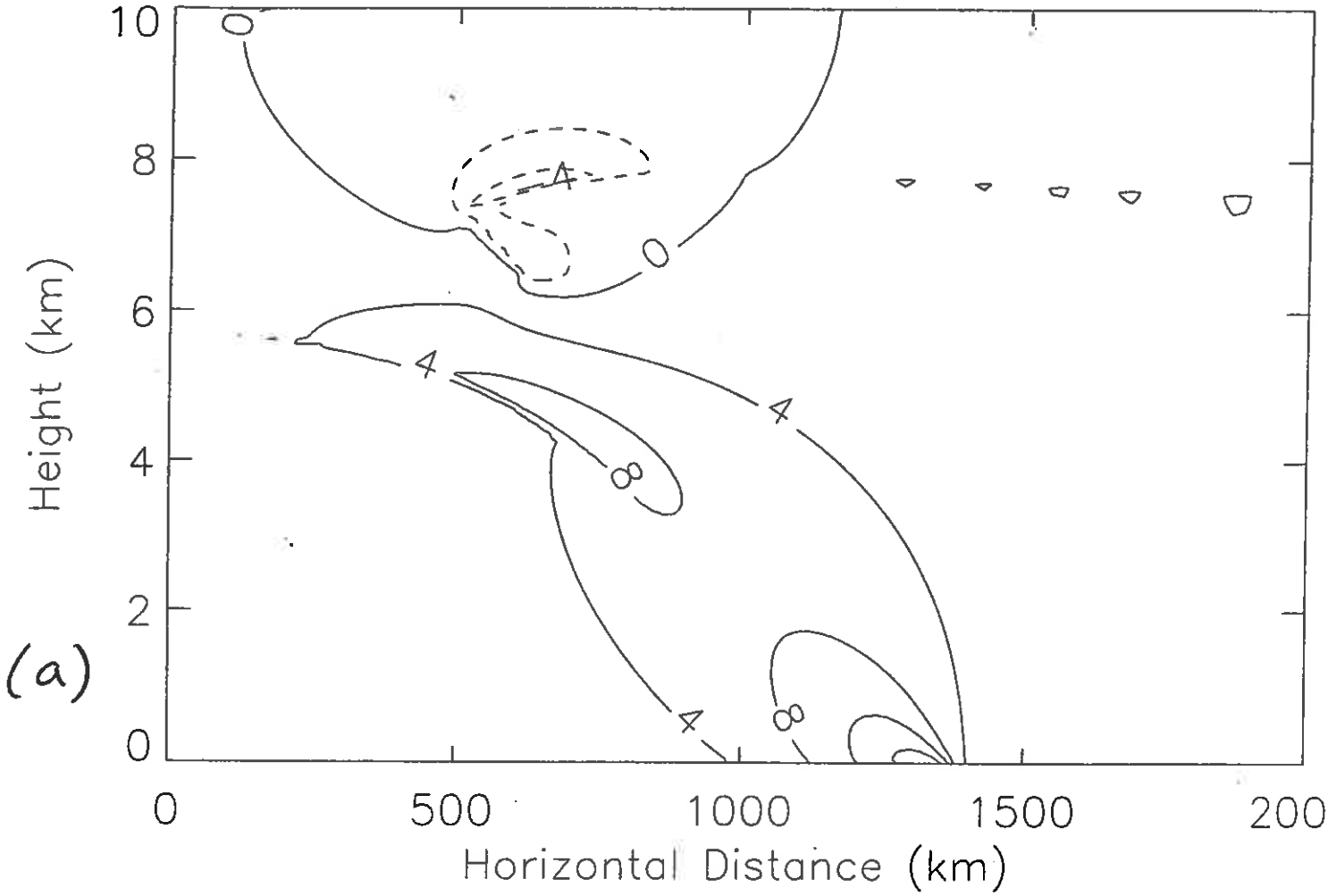
(a)
Height (km)
Horizontal Distance (km)
0
500
1000
1500
200
0
2
4
6
8
10
0
4
8

FIGURE 2

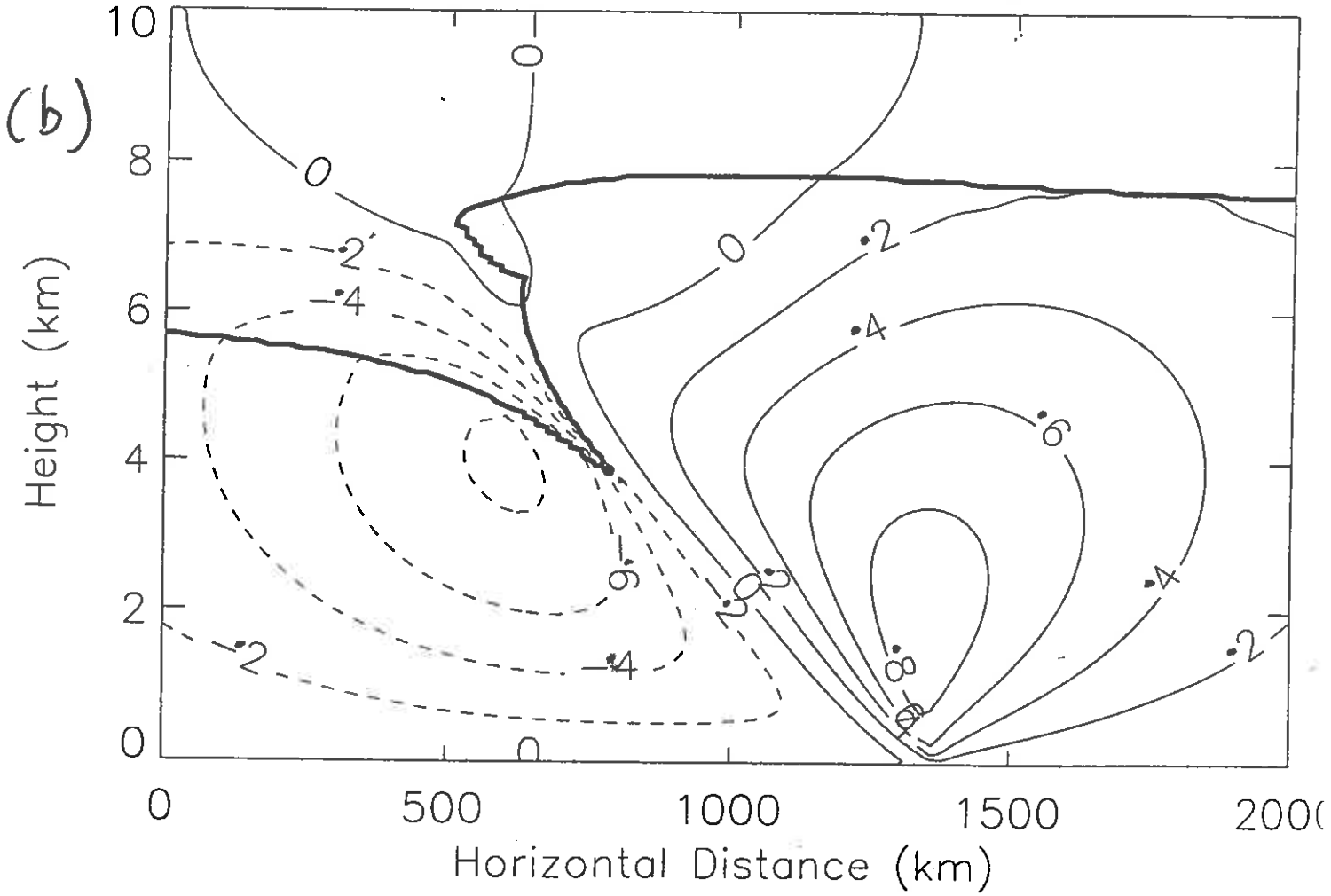
(b)
Height (km)
Horizontal Distance (km)
0
500
1000
1500
200(
0
2
4
6
8
10
0
2
4
6
8

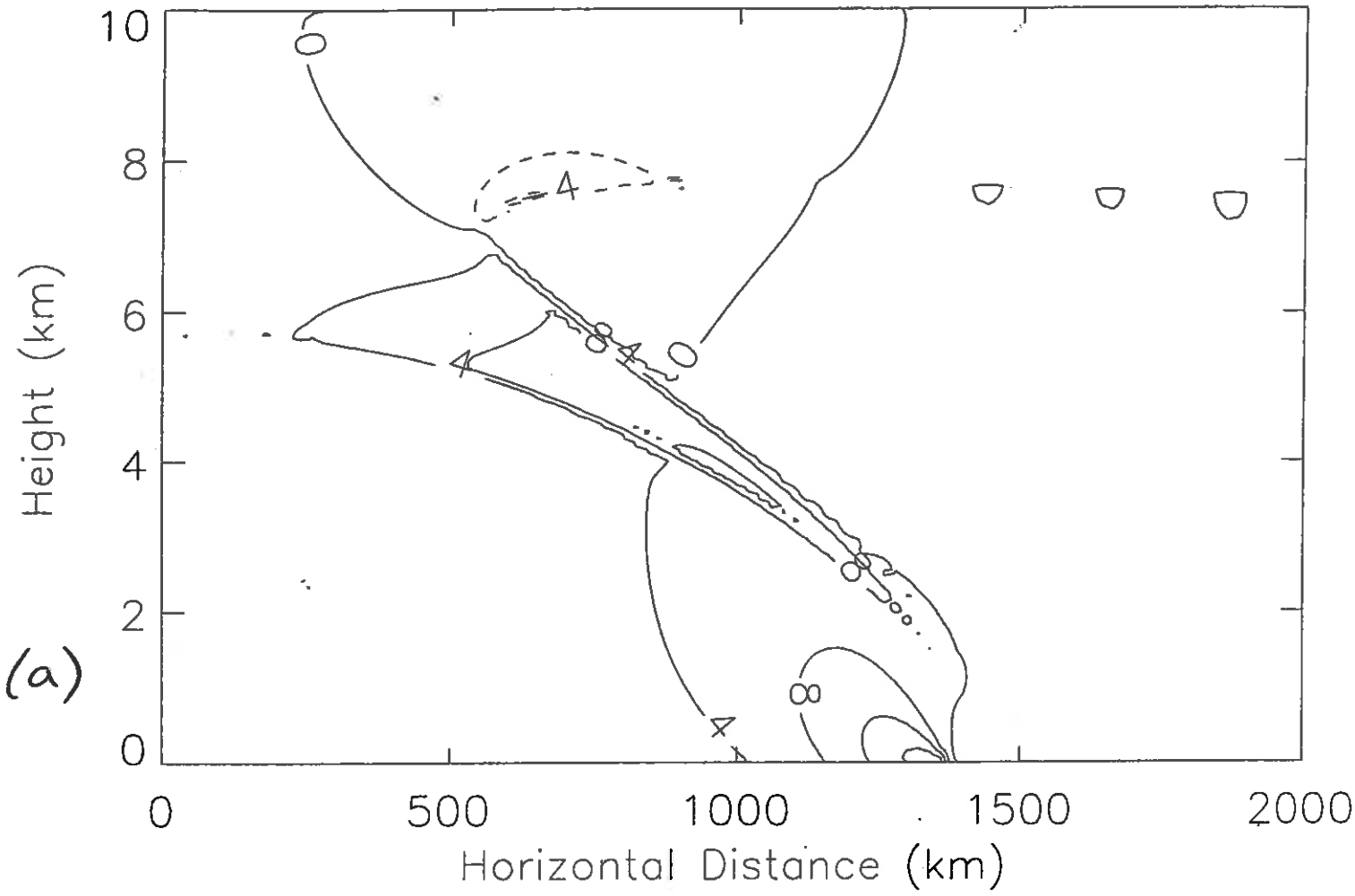
(a)
Height (km)
Horizontal Distance (km)
0
500
1000
1500
2000
0
2
4
6
8
10

FIGURE 3

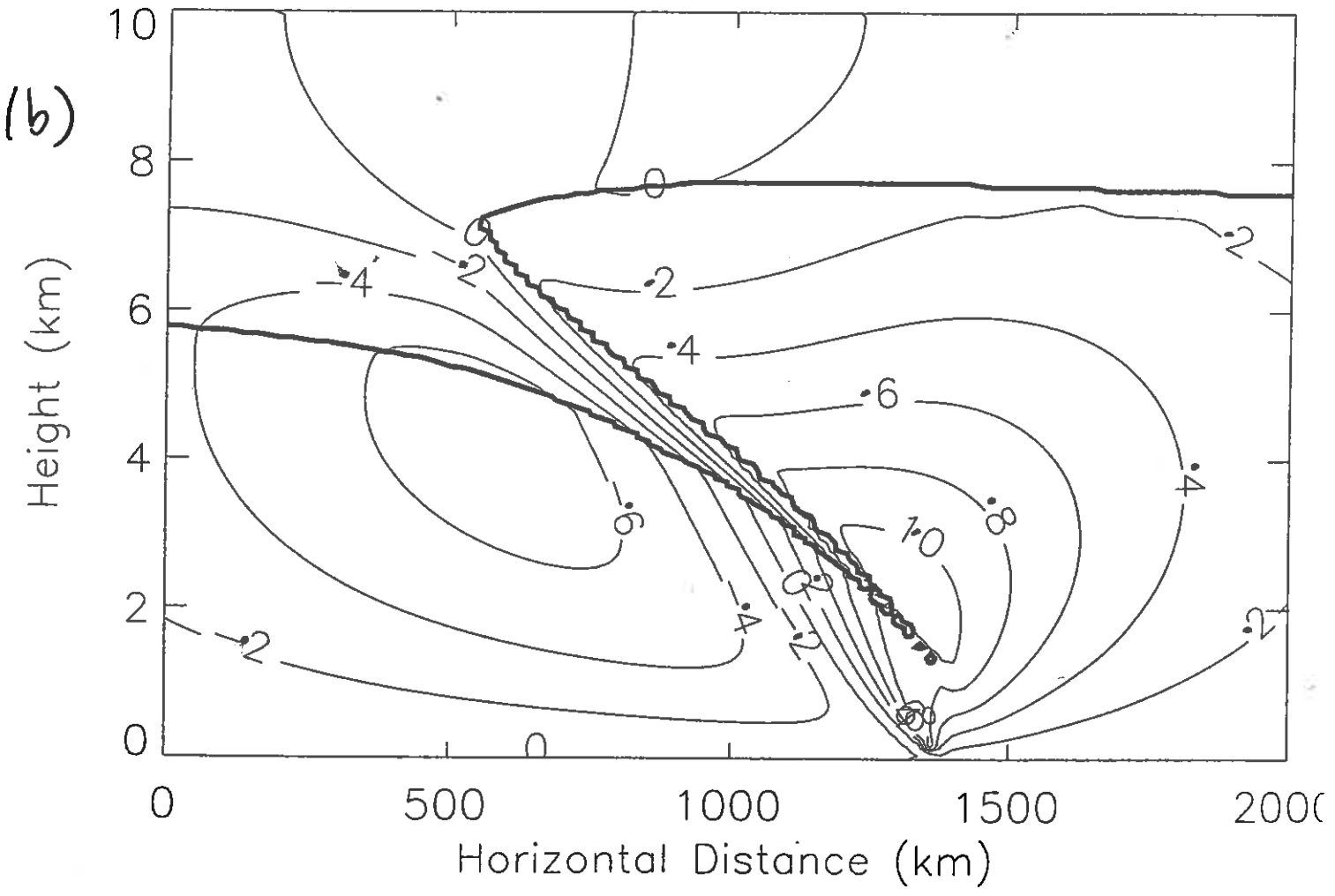
(b)
Height (km)
Horizontal Distance (km)
0
500
1000
1500
2000
0
2
4
6
8
10

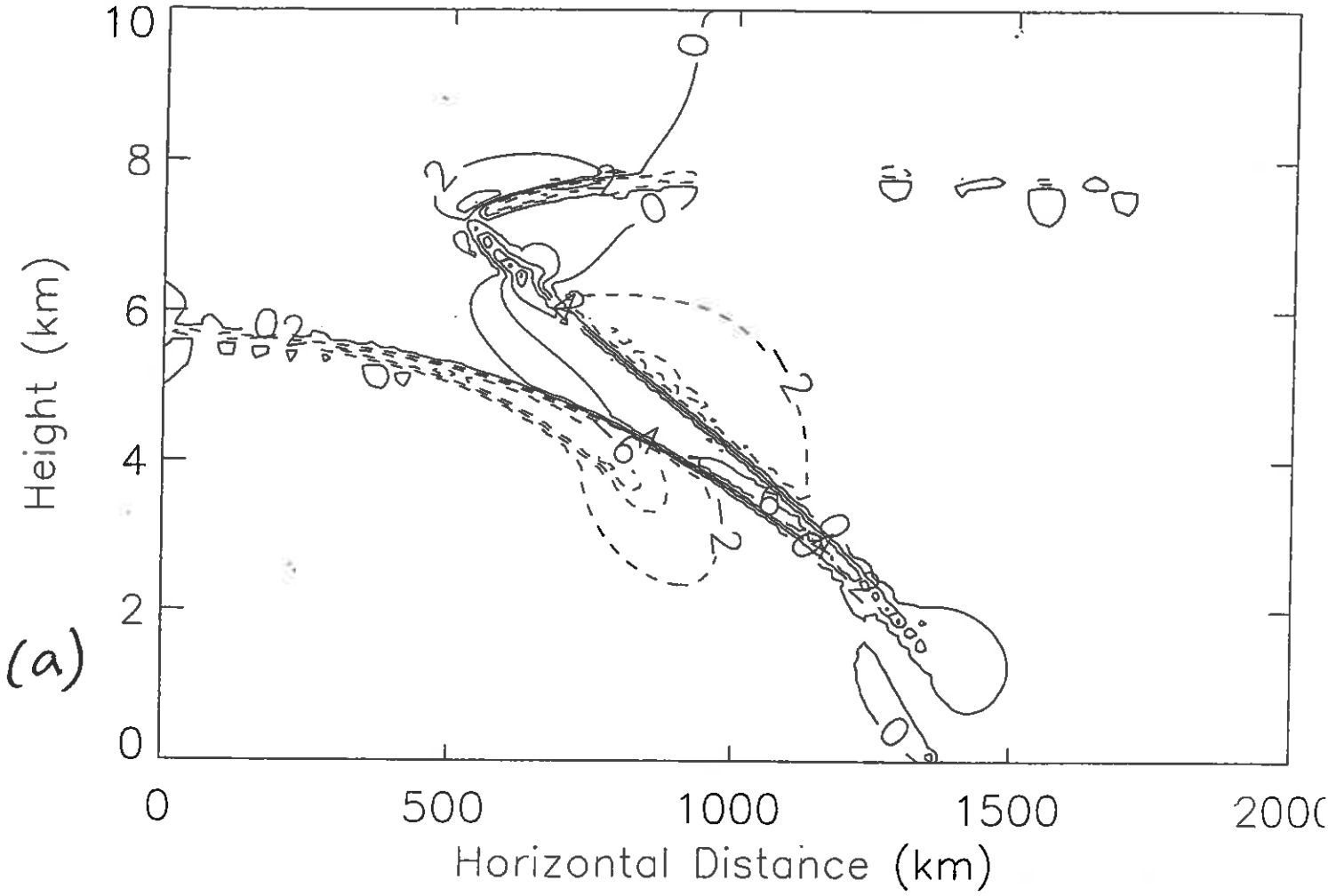
(a)
Height (km)
Horizontal Distance (km)
0
500
1000
1500
2000
0
2
4
6
8
10

FIGURE 4

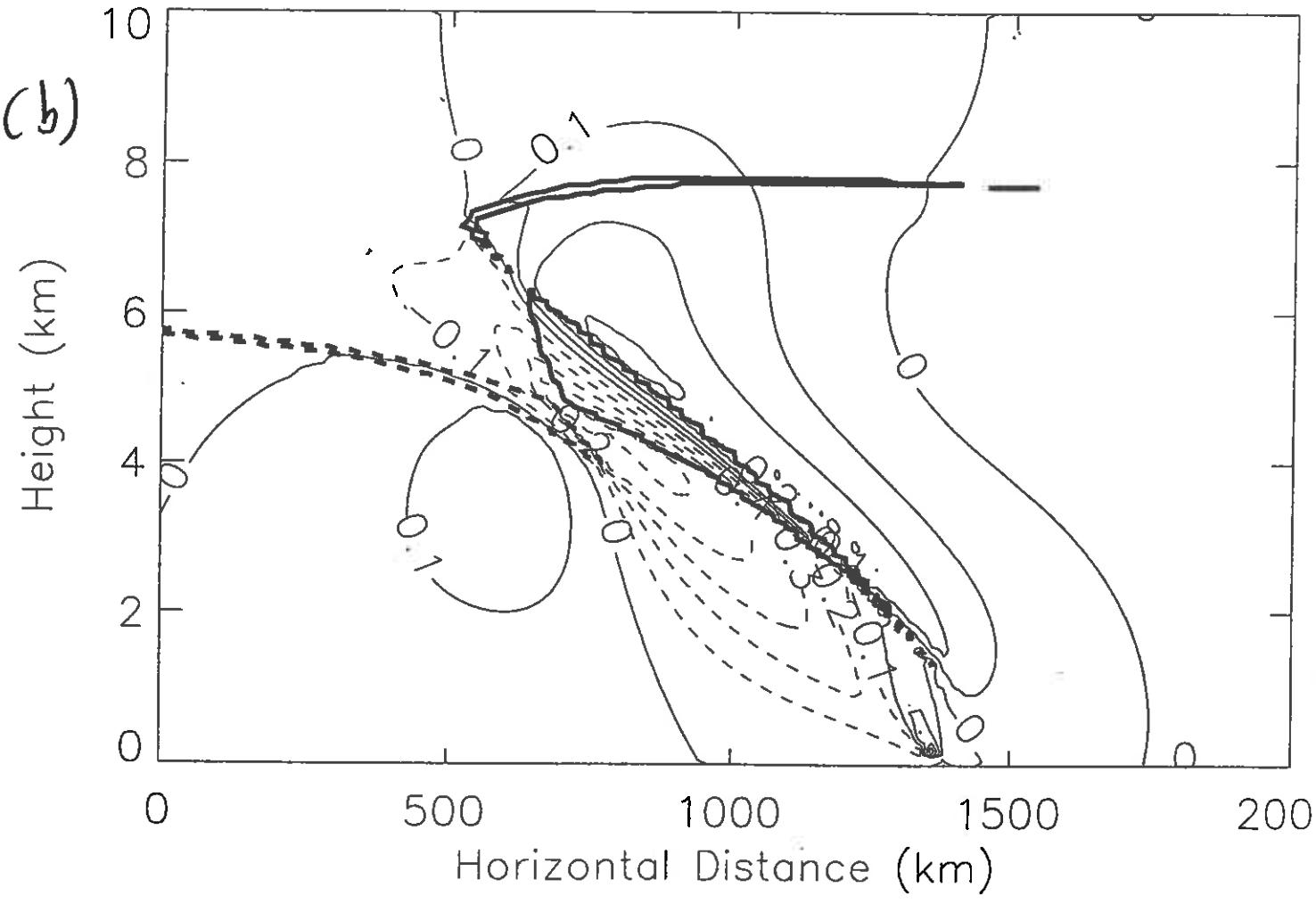
(b)
Height (km)
Horizontal Distance (km)
0
500
1000
1500
200
0
2
4
6
8
10

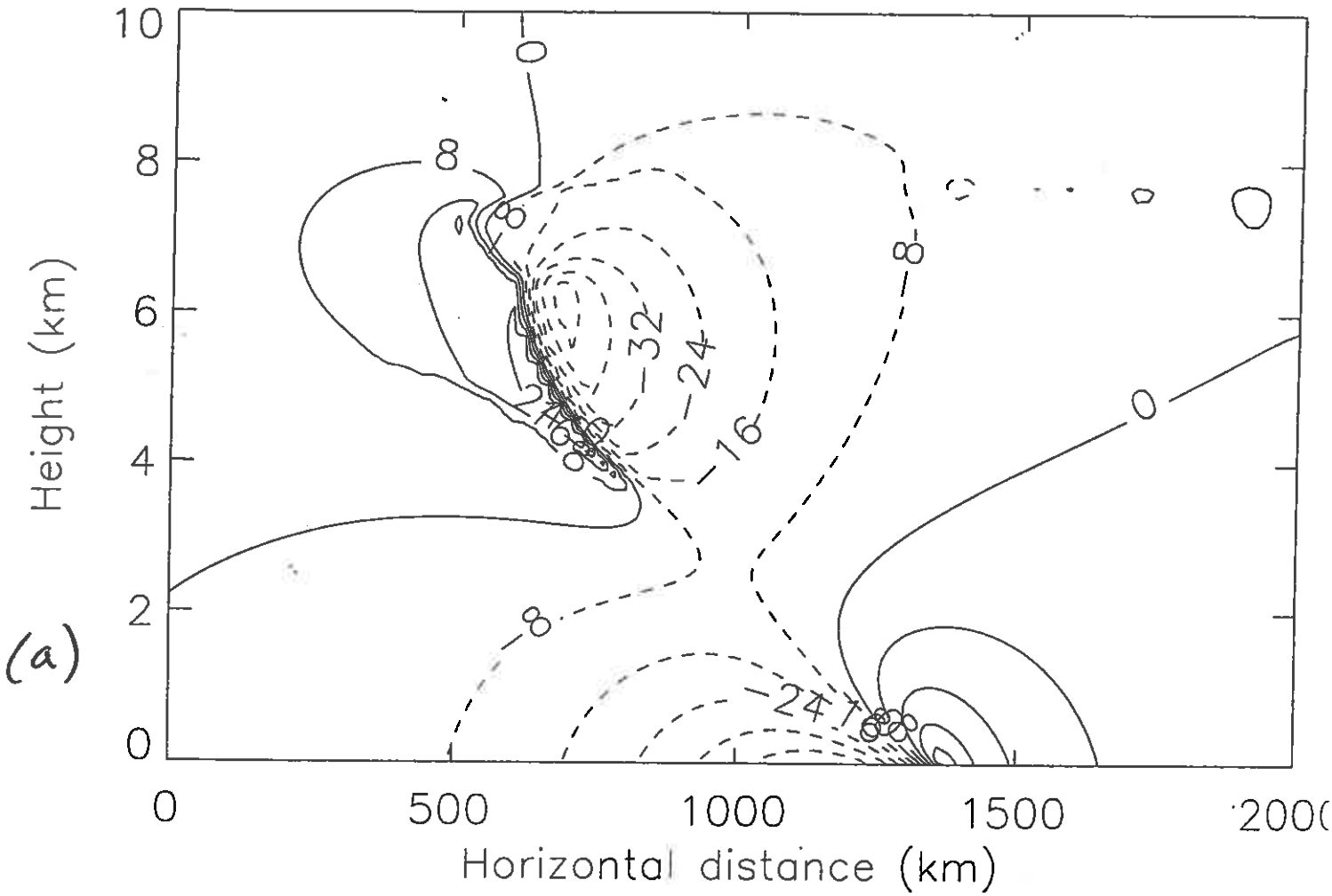
(a)
Height (km)
Horizontal distance (km)
0
500
1000
1500
2000
0
2
4
6
8
10
0
8
-8
-32
-24
-16
-24

FIGURE 5

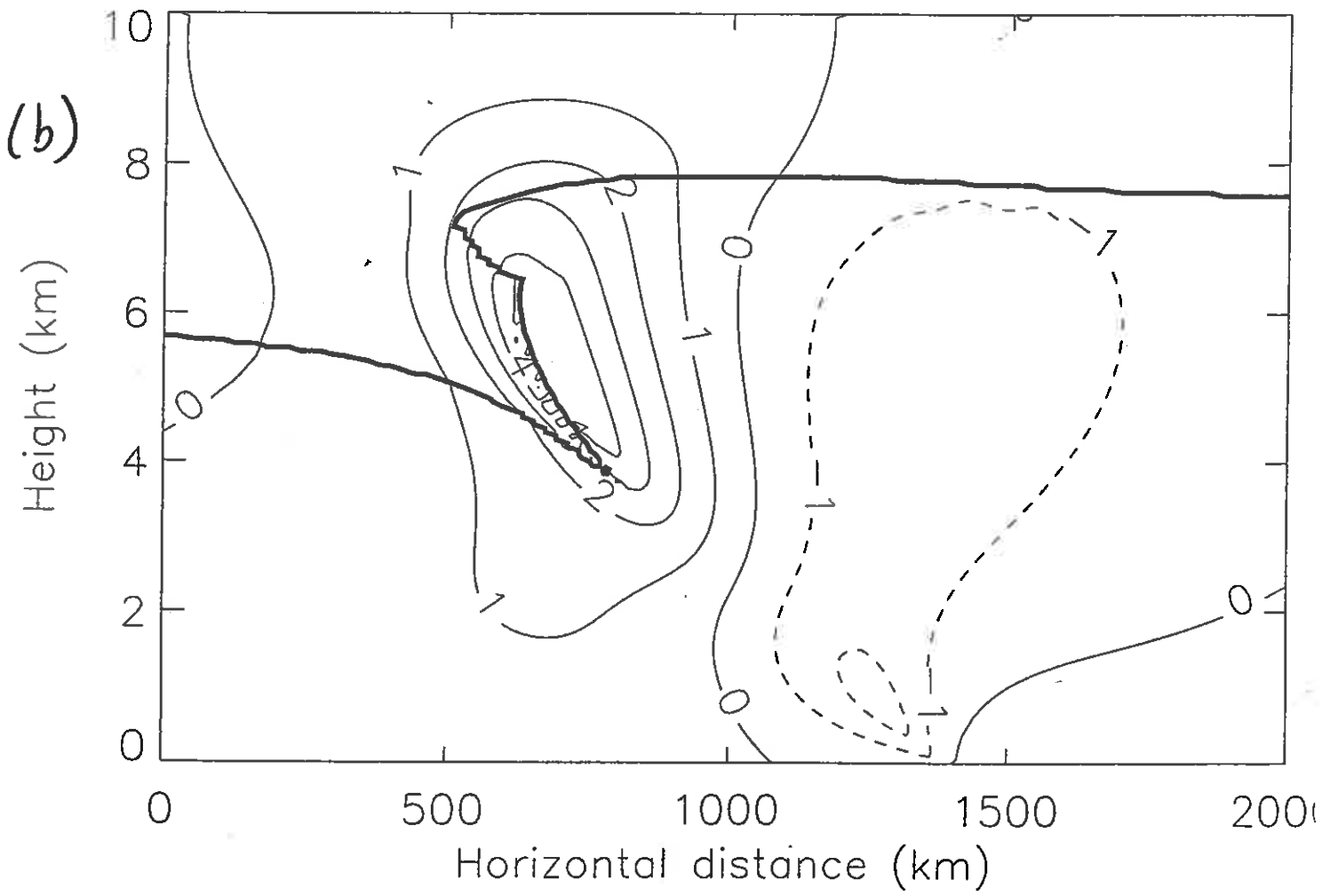
(b)
Height (km)
Horizontal distance (km)
0
500
1000
1500
2000
0
2
4
6
8
10
0
1
2
-1

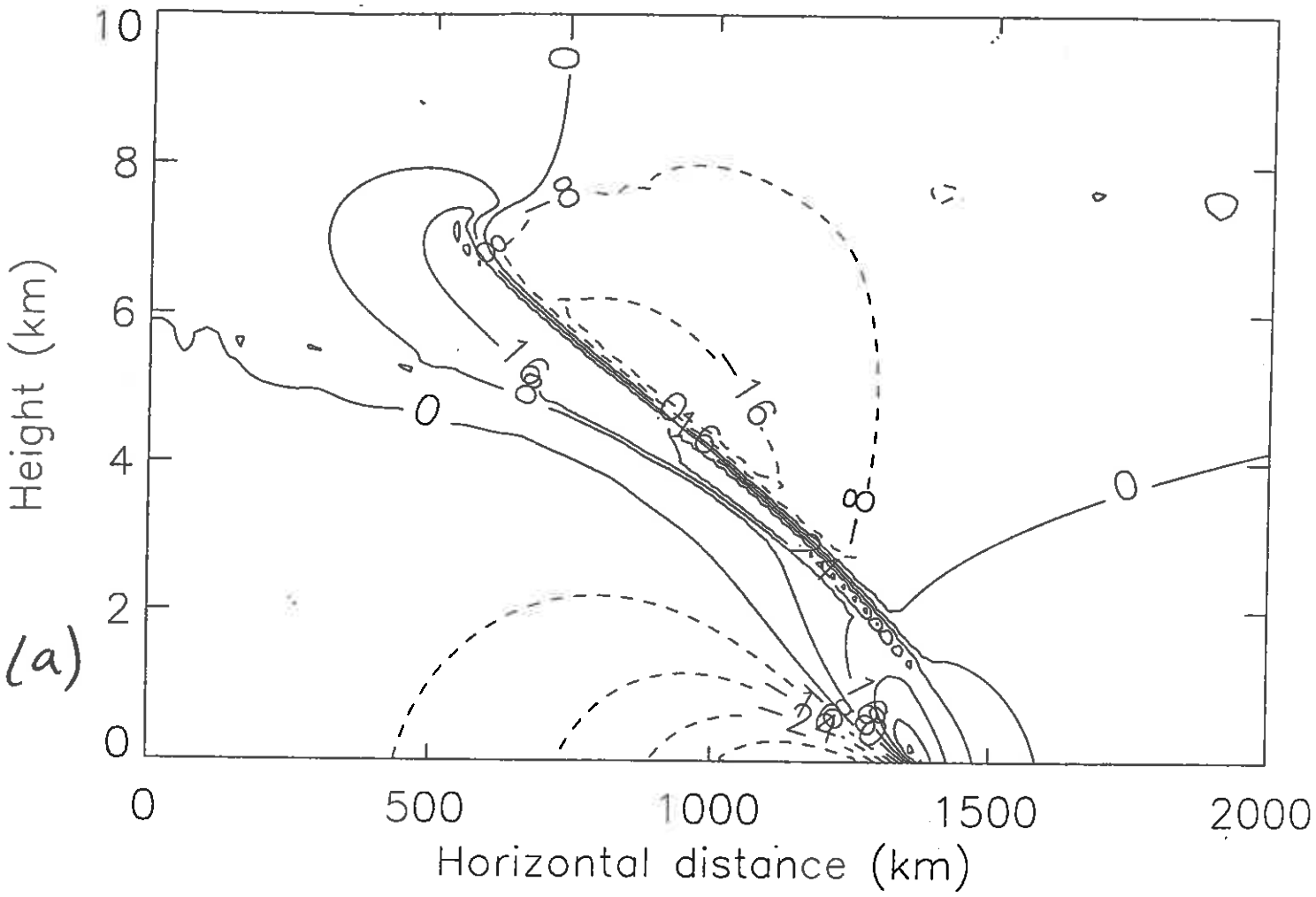
(a)
Height (km)
Horizontal distance (km)
0
500
1000
1500
2000
0
2
4
6
8
10

FIGURE 6

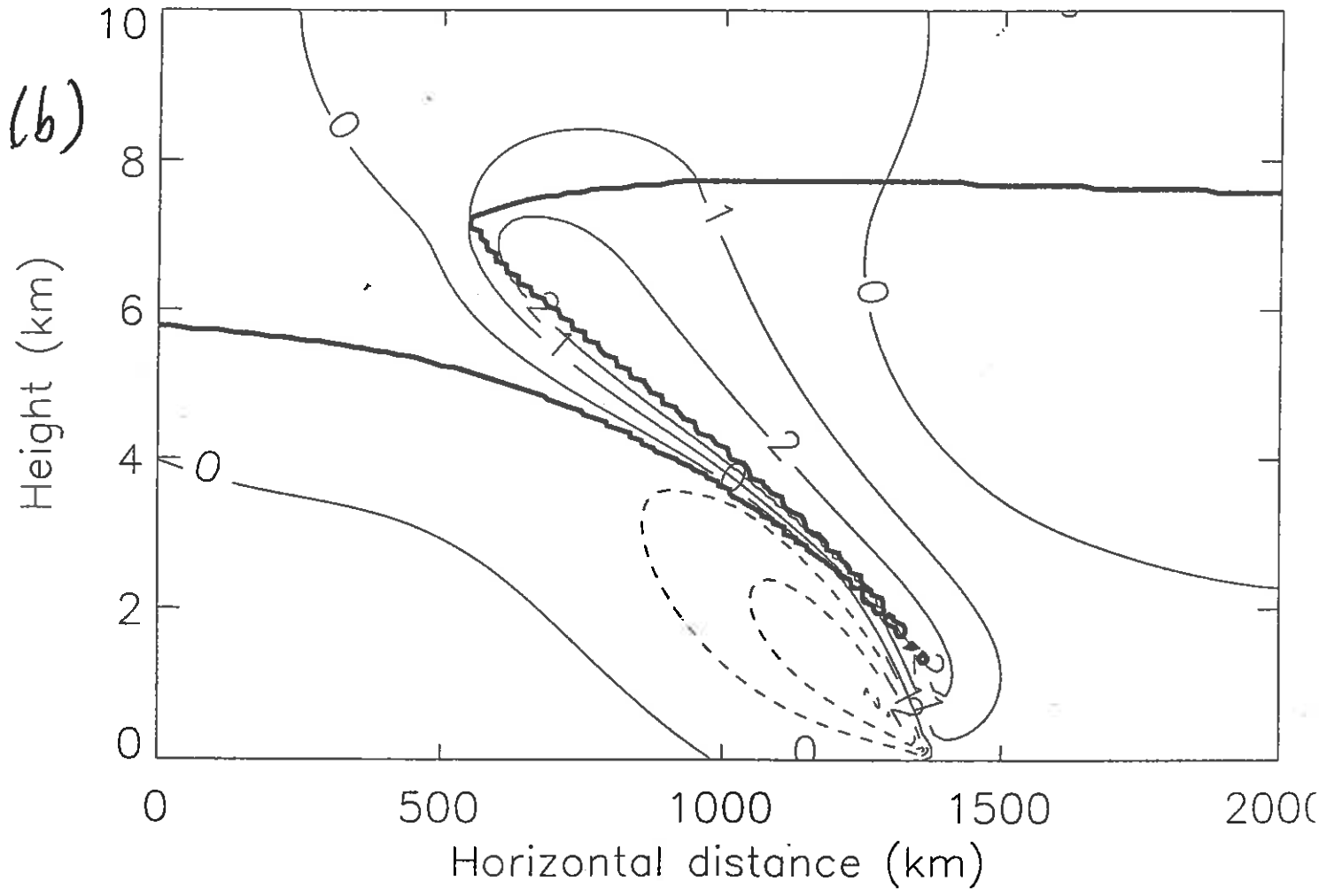
(b)
Height (km)
Horizontal distance (km)
0
500
1000
1500
2000
0
2
4
6
8
10

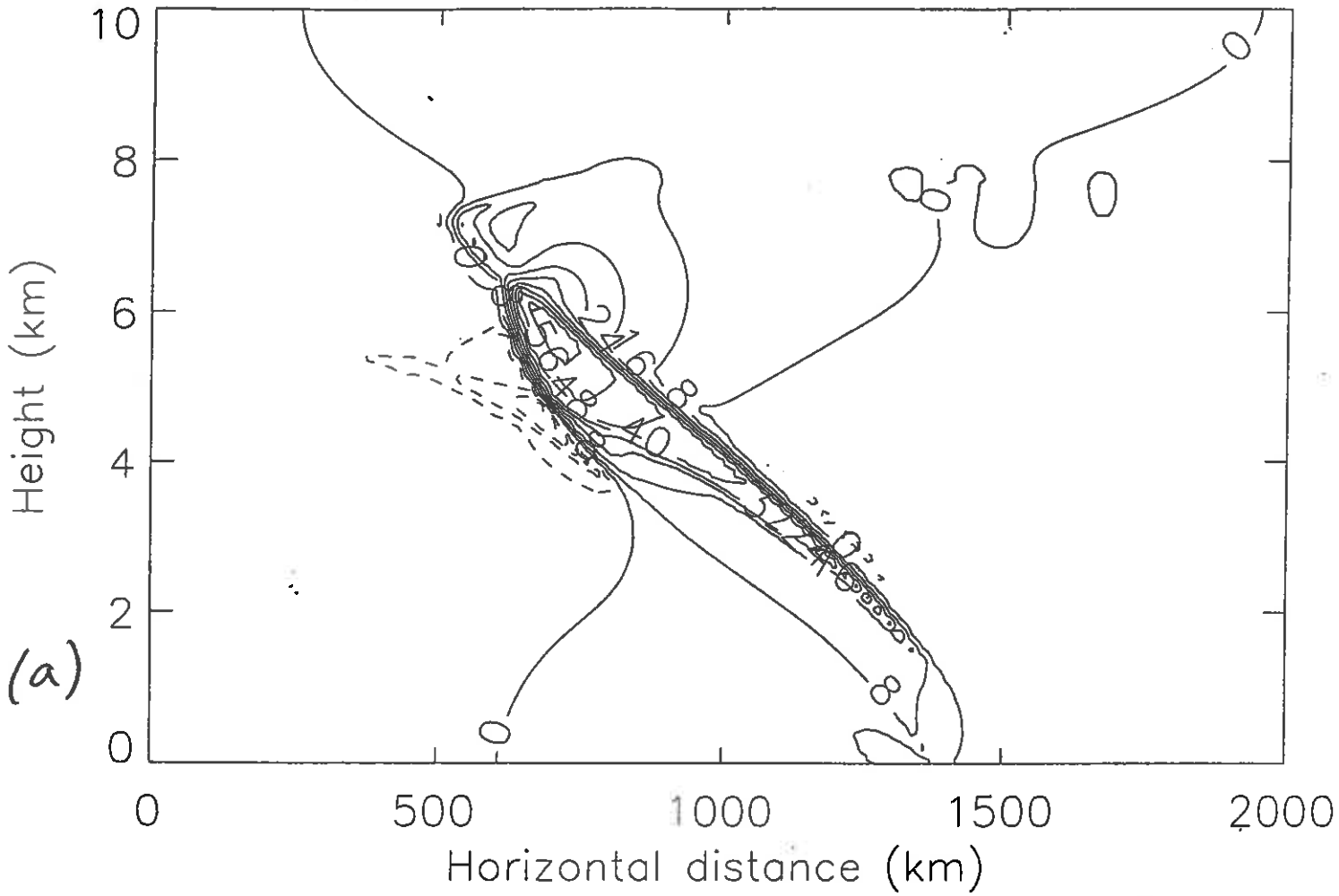
(a)
Height (km)
Horizontal distance (km)
0
2
4
6
8
10
0
500
1000
1500
2000

FIGURE 7

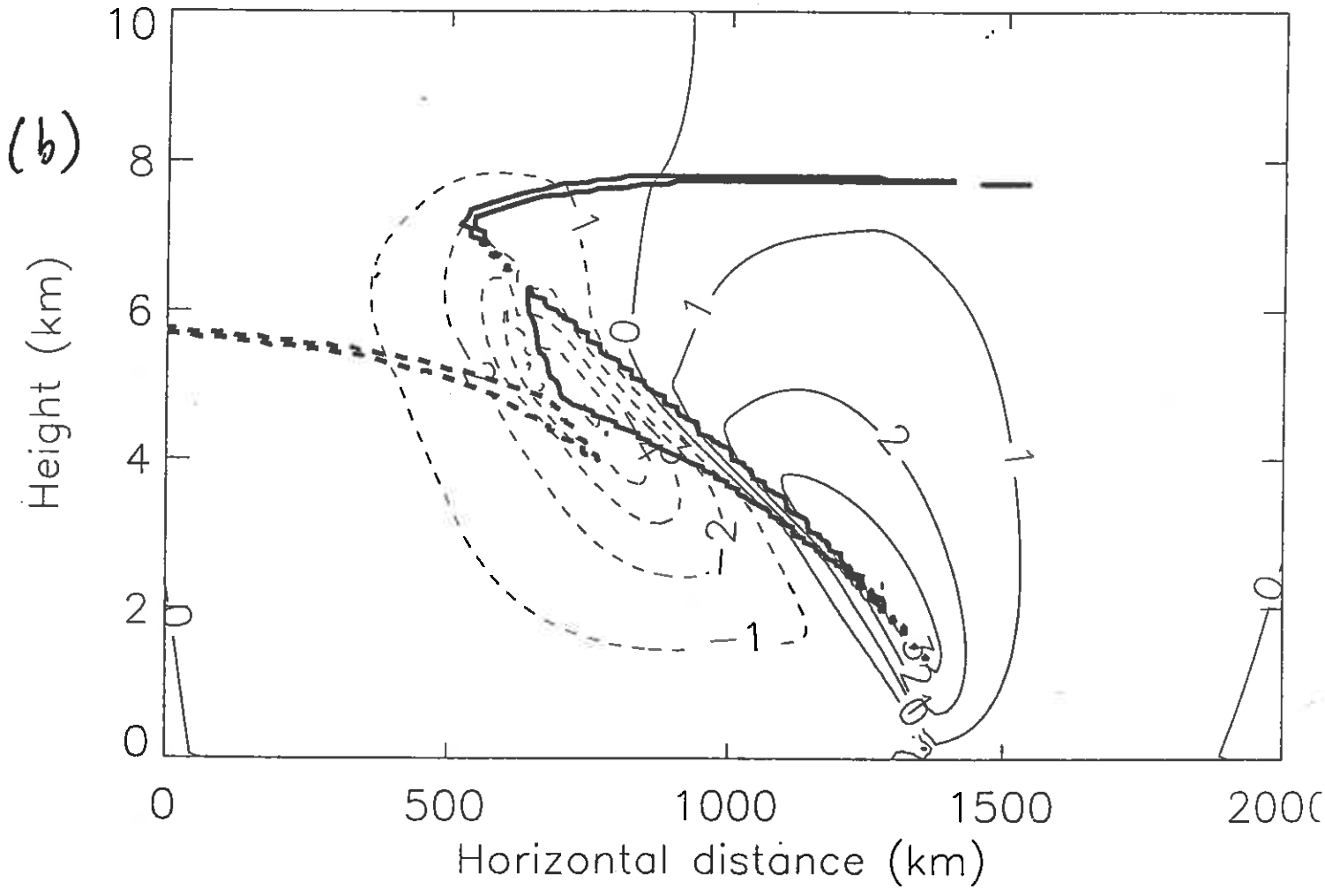
(b)
Height (km)
Horizontal distance (km)
0
2
4
6
8
10
0
500
1000
1500
2000

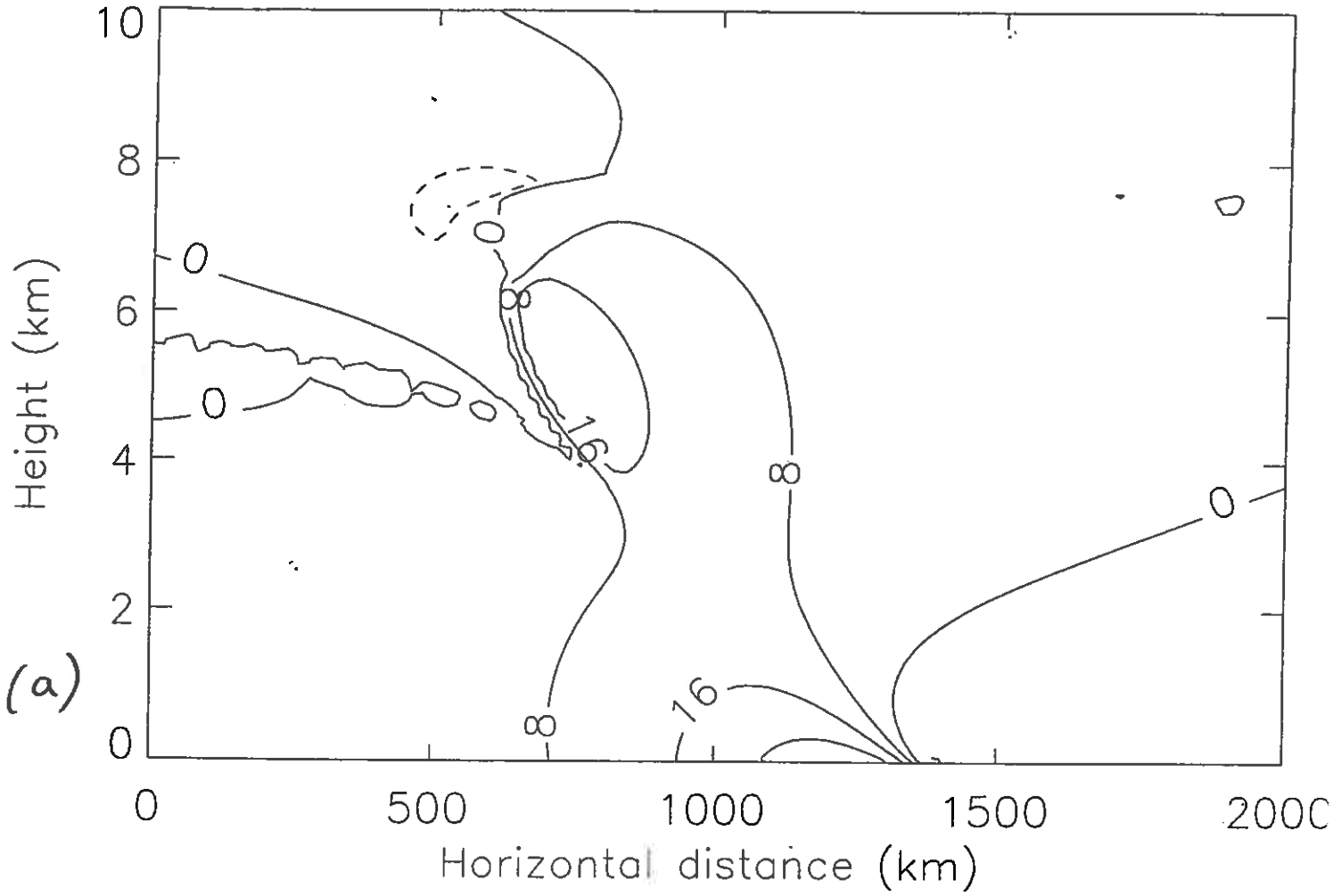
(a)
Height (km)
Horizontal distance (km)
0
500
1000
1500
2000
0
2
4
6
8
10
0
8
16

FIGURE 8

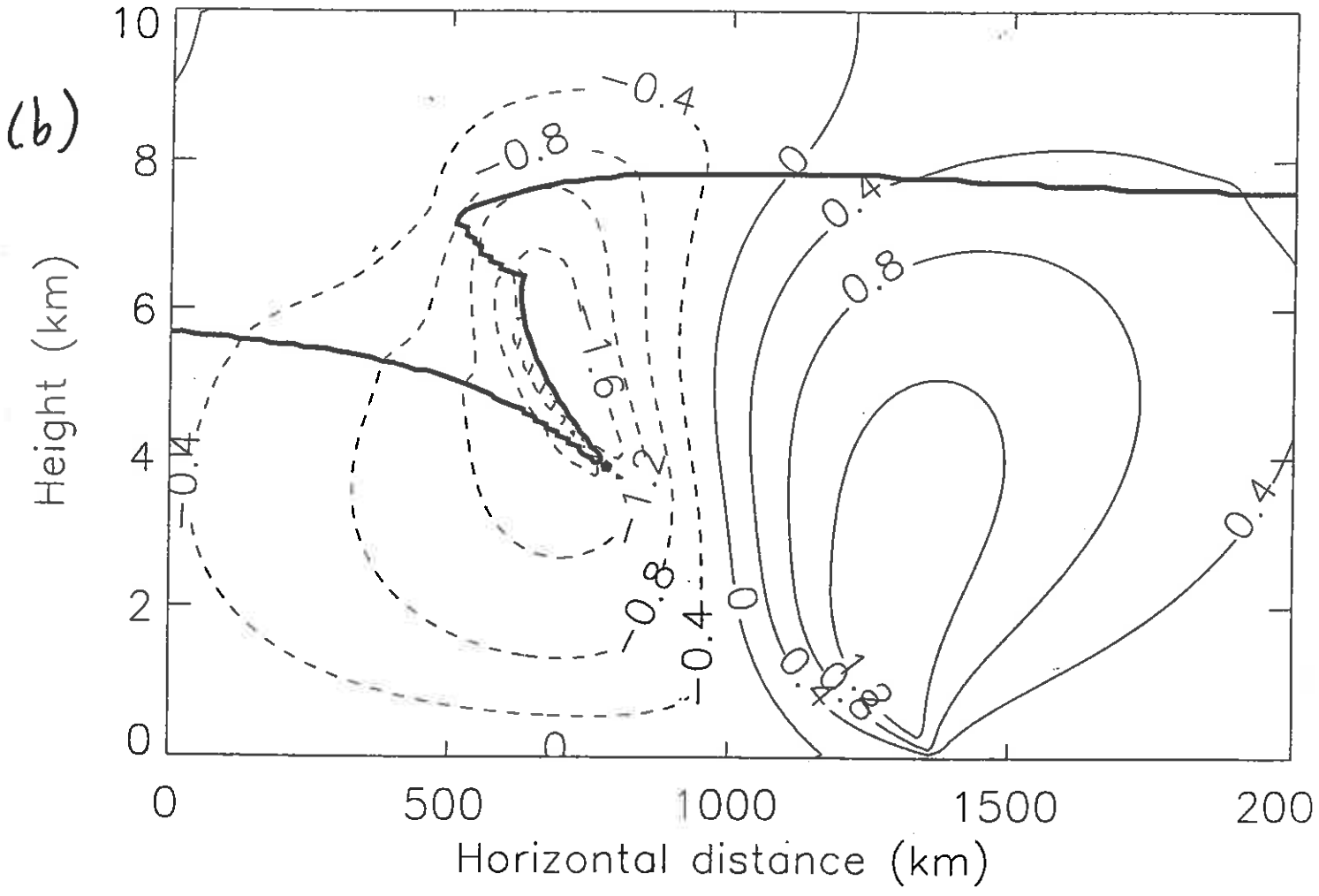
(b)
Height (km)
Horizontal distance (km)
0
500
1000
1500
200
0
2
4
6
8
10
-0.4
-0.8
-1.2
-1.6
0
0.4
0.8

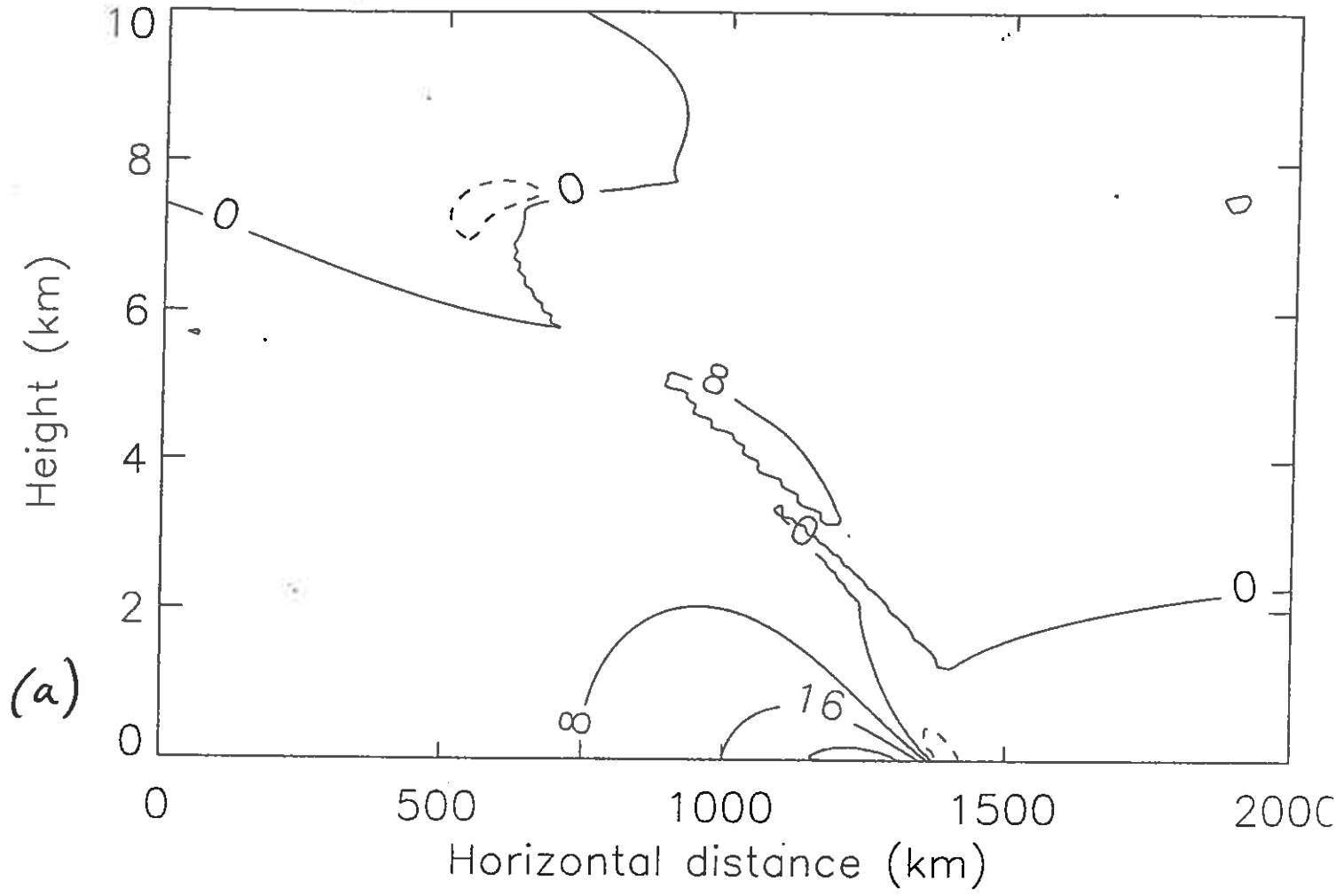
(a)
Height (km)
Horizontal distance (km)
0
500
1000
1500
2000
0
2
4
6
8
10
0
8
16

FIGURE 9

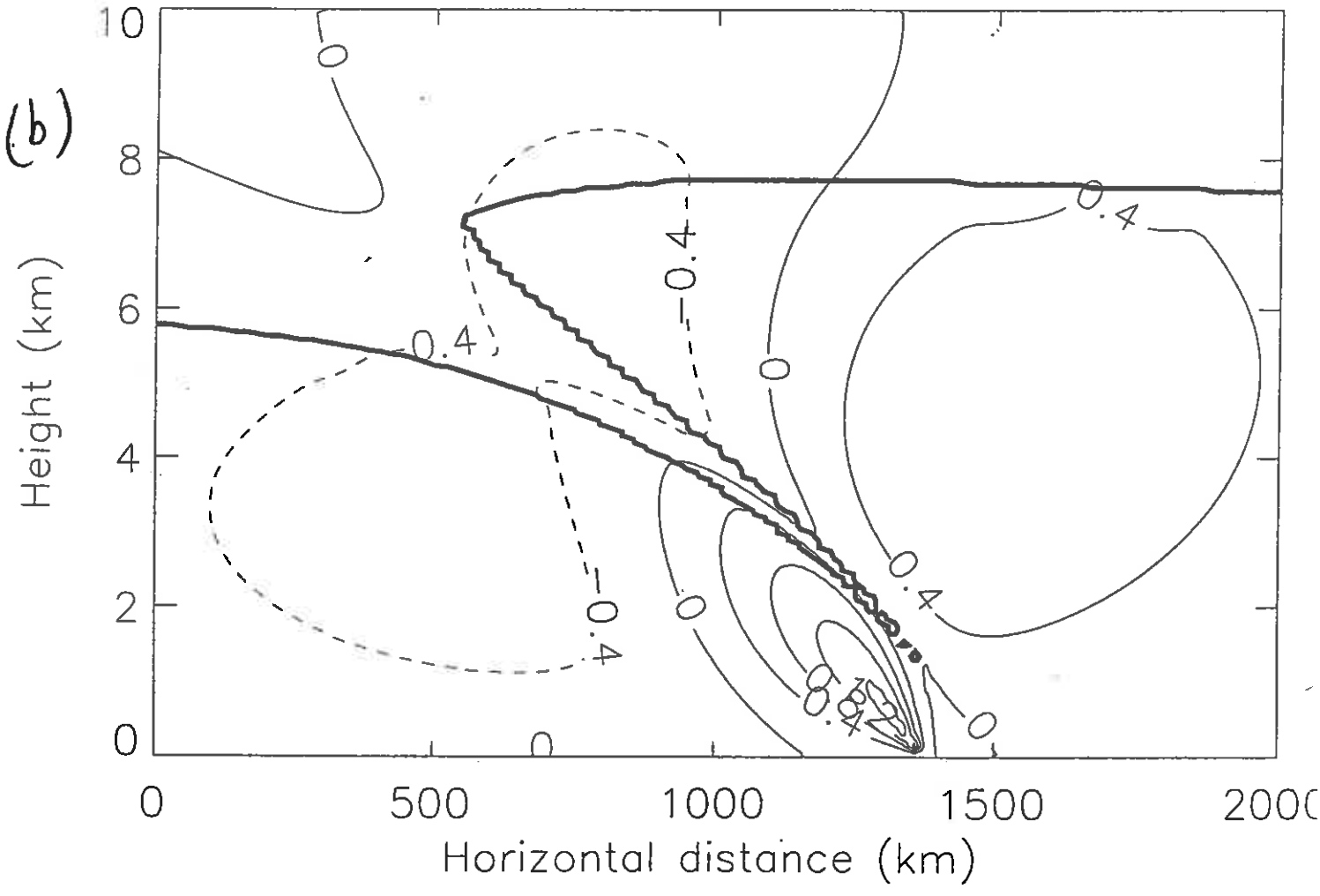
(b)
Height (km)
Horizontal distance (km)
0
500
1000
1500
2000
0
2
4
6
8
10
0.4
-0.4

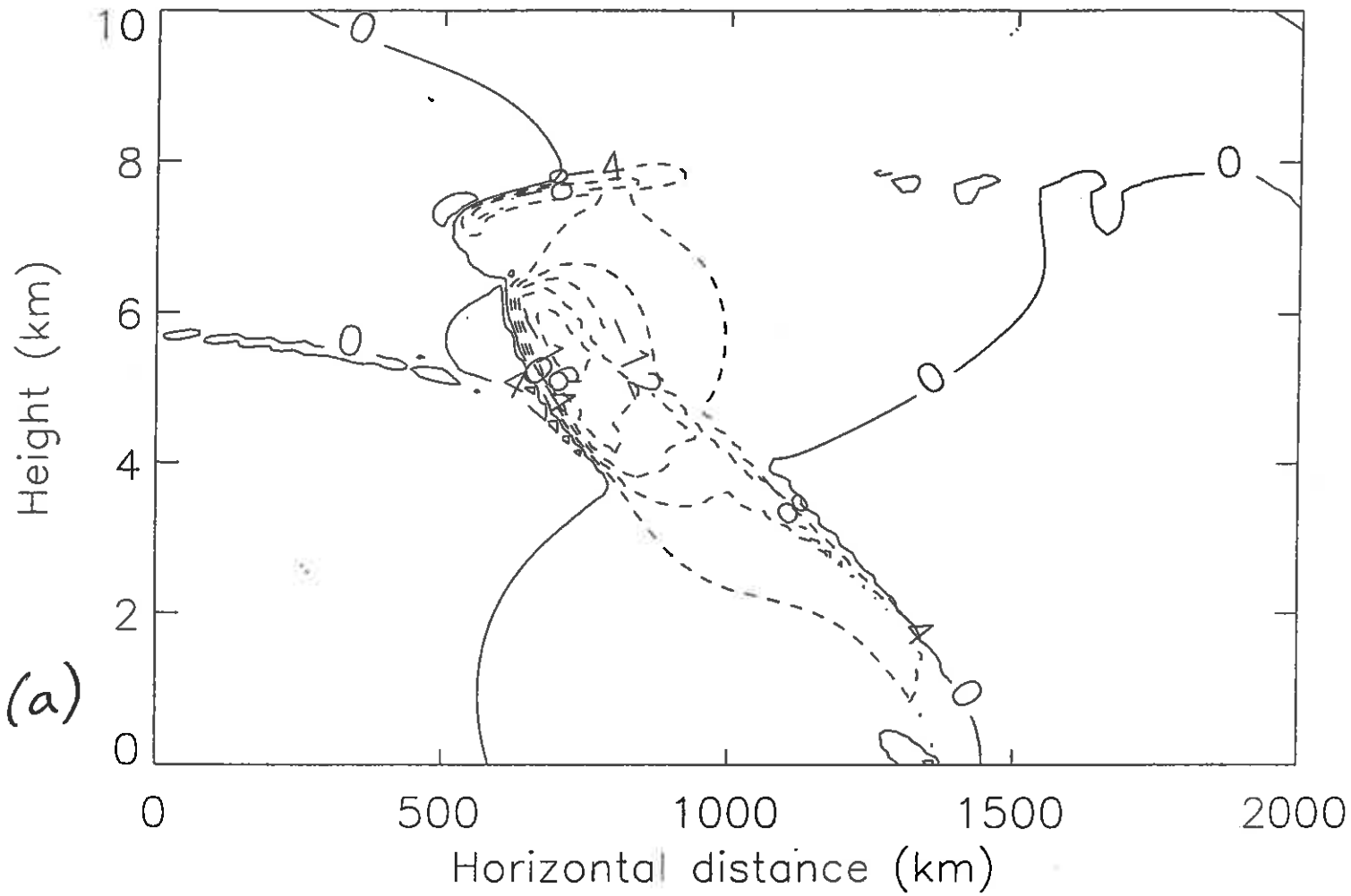
(a)
Height (km)
Horizontal distance (km)
0
500
1000
1500
2000
0
2
4
6
8
10
0
4
8
12
16

FIGURE 10

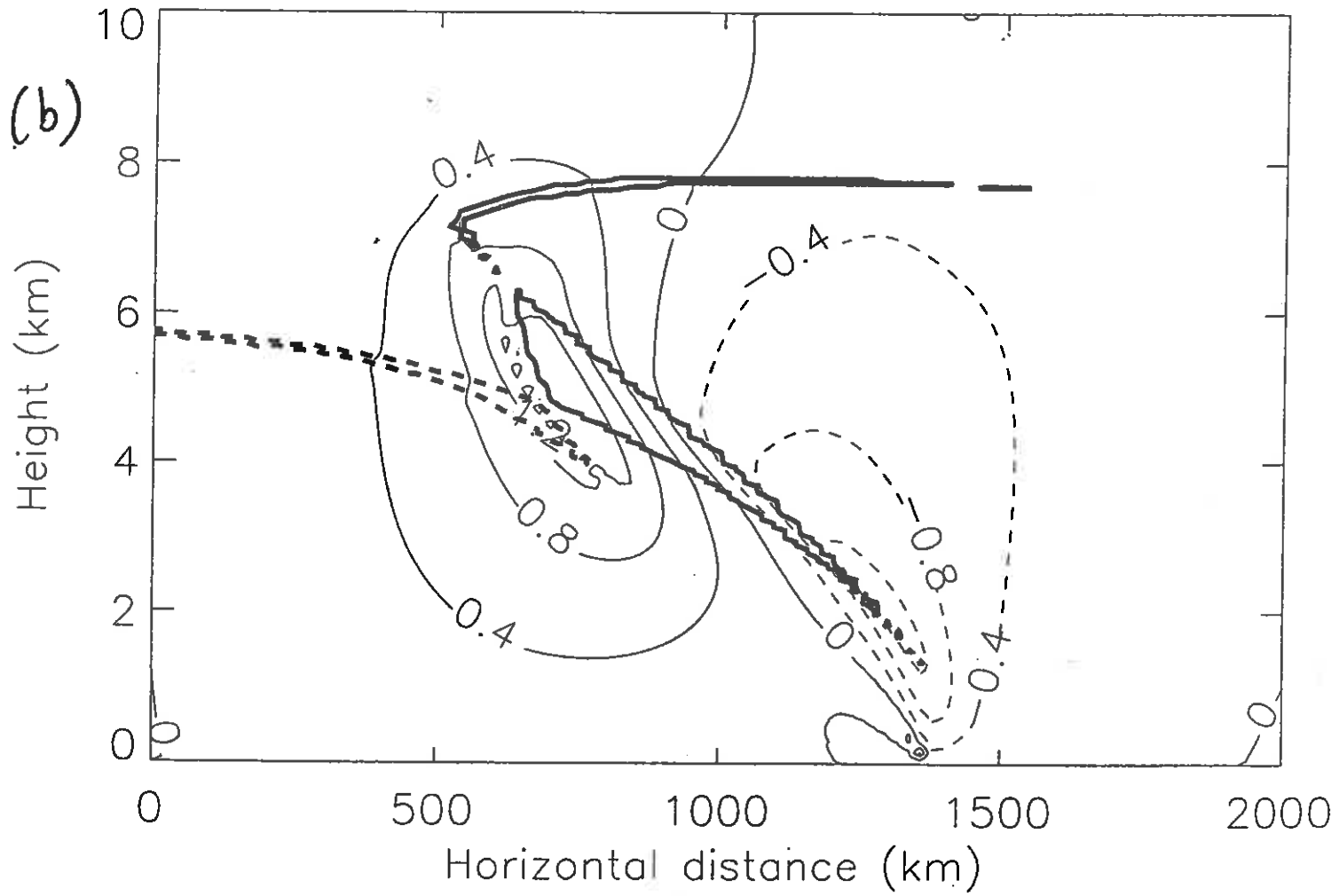
(b)
Height (km)
Horizontal distance (km)
0
500
1000
1500
2000
0
2
4
6
8
10
0.4
0
0.8
1.2

CURRENT JCMM INTERNAL REPORTS

This series of JCMM Internal Reports, initiated in 1993, contains unpublished reports and also versions of articles submitted for publication. The complete set of Internal Reports is available from the National Meteorological Library on loan, if required.

1. **Research Strategy and Programme**
   K A Browning et al
   January 1993

2. **The GEWEX Cloud System Study (GCSS)**
   GEWEX Cloud System Science Team
   January 1993

3. **Evolution of a mesoscale upper tropospheric vorticity maximum and comma cloud from a cloud-free two dimensional potential vorticity anomaly**
   K A Browning
   January 1993

4. **The Global Energy and Water Cycle**
   K A Browning
   July 1993

5. **Structure of a midlatitude cyclone before occlusion**
   K A Browning and N Roberts
   July 1993

6. **Development in Systems and Tools for Weather Forecasting**
   K A Browning and G Szejwach
   July 1993

7. **Diagnostic study of a narrow cold frontal rainband and severe winds associated with a stratospheric intrusion**
   K A Browning and R Reynolds
   August 1993

8. **Survey of perceived priority issues in the parametrizations of cloud-related processes in GCMs**
   K A Browning
   September 1993

9. **The Effect of Rain on Longwave Radiation**
   I Dharssi
   September 1993

10. **Physical Cloud Microprocesses - A Description of the Parametrization used in the Large Eddy Model**
H Swann
July 1994

11. **An Appreciation of the Meteorological Research of Ernst Kleinschmidt**
A J Thorpe
May 1992

12. **Potential Vorticity of Flow Along the Alps**
A J Thorpe, H Volkert and Dietrich Heimann
August 1992

13. **The Representation of Fronts**
A J Thorpe
January 1993

14. **A Parametrization Scheme for Symmetric Instability: Test for an Idealised Flow**
C S Chan and A J Thorpe
February 1993

15. **The Fronts 92 Experiment: a Quicklook Atlas**
Edited by T D Hewson
November 1993

16. **Frontal wave stability during moist deformation frontogenesis**
Part 1. Linear wave dynamics
C H Bishop and A J Thorpe
May 1993

17. **Frontal wave stability during moist deformation frontogenesis**
Part 2. The suppression of non-linear wave development
C H Bishop and A J Thorpe
May 1993

18. **Gravity waves in sheared ducts**
C Bishop and A J Thorpe
November 1993

19. **Potential Vorticity and the Electrostatics Analogy: Quasi - Geostrophic Theory**
C Bishop and A J Thorpe
November 1993

20. **Recent Advances in the Measurement of Precipitation by Radar**
A J Illingworth - April 1993

21. **Micro-Physique et Givrage. Cloud Microphysics and Aircraft Icing**
A J Illingworth May 1993

22. **Differential Phase Measurements of Precipitation**
M Blackman and A J Illingworth
May 1993

23. **Estimation of Effective Radius of Cloud Particles from the Radar Reflectivity**
N I Fox and A J Illingworth
May 1993

24. **A Simple Method of Dopplerising a Pulsed Magnetron Radar**
A Hau, A J Illingworth and J Eastment
November 1993

25. **Radiation and Polar Lows**
George C Craig
February 1994

26. **Collected preprints submitted to the International Symposium on the Life Cycles of Extratropical Cyclones; Bergen, Norway, 27 June - 1 July 1994**
April 1994

27. **Convective Frontogenesis**
Douglas J Parker and Alan J Thorpe
April 1994

28. **Improved Measurement of the Ice Water Content in Cirrus Using a Total Water Evaporator**
Philip R A Brown and Peter N Francis
April 1994

29. **Mesoscale Effects of a Dry Intrusion within a Vigorous Cyclone**
K A Browning and B W Golding
April 1994

30. **GEWEX Cloud System Study, Science Plan**
May 1994

31. **Parametrization of Momentum Transport by Convectively Generated Gravity Waves**
R Kershaw
February 1995

32. **Mesoscale Modelling Newsletter No 5**
May 1994

33. **Observations of the mesoscale sub-structure in the cold air of a developing frontal cyclone**
K A Browning, S A Clough, C S A Davitt, N M Roberts and T D Hewson
May 1994

34. **Longwave Radiative Forcing of a Simulated Tropical Squall Line**
Imtiaz Dharssi
July 1994

35. **On the nature of the convective circulation at a kata-cold front**
K A Browning
September 1994

36. **Collective preprints of papers submitted to the COST-75 International Seminar on Advanced Weather Radar Systems, Brussels, 20-23 September 1994**
November 1994

37. **Use of satellite imagery to diagnose events leading to frontal thunderstorms: Parts 1 and 11 of a case study**
K A Browning and N M Roberts
November 1994

38. **The role of spaceborne millimetre-wave radar in the global monitoring of ice cloud**
P R A Brown, A J Illingworth, A J Heymsfield, G M McFarquahar, K A Browning and M Gosset
December 1994

39. **Potential Vorticity Inversion**
Michael Ziemianski
October 1994

40. **Theory of mature tropical cyclones; a comparison between Kleinschmidt (1951) and Emanuel (1986)**
Suzanne L Gray
December 1994

41. **Dispersion and removal of pollutants during the passage of an atmospheric frontal System**
N R Gimson
December 1994

42. **The role of snow sublimation in frontogenesis**
D J Parker and A J Thorpe
December 1994

43. **Potential vorticity and the electrostatics Analogy: Ertel- Rossby formulation**
A J Thorpe and C H Bishop
December 1994

44. **Mesoscale aspect of extratropical cyclones: an observational perspective**
K A Browning
January 1995

45. **A Polar Low Outbreak: Evolution and Mesoscale Structures**
T D Hewson, G C Craig and C Claud
February 1995

46. **Generation of near-surface gusts of deep convection**
K Nakamura and R Kershaw
April 1995

47. **Attribution Concepts applied to the Omega Equation**
S A Clough, C S A Davitt and A J Thorpe
June 1995

48. **Parametrization of mixed-phase cloud and precipitation**
Susan P Ballard and M Gerard Hutchinson
June 1995

49. **Short-range forecasting of stratocumulus: Initialization Prediction**
Susan Ballard, Simon D Jackson and B Macpherson
June 1995

50. **Contributions of the JCMM/Dept of Meteorology Radar Group to the 27th AMS Radar Meteorology Conference, Vail October 1995**
June 1995

51. **Cold Pools in Shear**
Douglas J Parker
September 1995

52. **High-resolution analysis of frontal fracture**
K A Browning, S P Ballard and C S A Davitt
September 1995

53. **The Albedo of Broken Cloud Fields: Calculations using a modified two stream radiation code**
Imtiaz Dharssi and Roy Kershaw
October 1995

54. **Parametrization of momentum transport by convection. I: Theory and cloud modelling results**
P Kershaw and D Gregory
November 1995

55. **Variation of frontal structure along a cold front**
K A Browning and N M Roberts
November 1995

56. **Secondary Frontal Waves**
Douglas Parker
December 1995

57. **Objective Fronts**
T D Hewson
March 1996

58. **Mesoscale analysis of the activation of a cold front during cyclogenesis**
K A Browning, N M Roberts and A J Illingworth
June 1996

59. **Investigation of Different Representations of Rain in a 1-d Evaporation Model**
H Swann
May 1996

60. **Parametrization of diabatic processes in the inversion of the omega-equation**
M Athanassiadou and A J Thorpe

61. **The Role of the Environmental Flow in the Development of Secondary Frontal Cyclones**
I A Renfrew, A J Thorpe and A Joly
June 1996

62. **Consequences of the geostrophic momentum approximation on barotropic instability**
S Malardel, A J Thorpe and A Joly
June 1996

63. **Contributions to the AMS/RMS Conference on Mesoscale Processes**
Reading, 9-13 September 1996

64. **Vorticity and Potential Vorticity in Stratified Flows Interacting with an Isolated Obstacle**
Jorge A Gutierrez and A J Thorpe
September 1996

65. **Triple Point Development: Two Case Studies**
Douglas Parker
September 1996

66. **Radar observations of wind-shear splitting within evolving atmospheric Kelvin-Helmholtz billows**
D Chapman and K A Browning
April 1997

67. **Cold Frontal Structure derived from radar wind profilers**
K A Browning, D Jerrett, J Nash, T Oakley, N M Roberts
May 1997

68. **The dry intrusion and its effect on the frontal, cloud and precipitation structure of extratropical cyclones**
K A Browning - Text of invited special lecture at the Spring Conference of the Meteorological Society of Japan, University of Tsukuba, 22 May 1997

69. **Met. Office Unified Model data, diagnostic graphics programs, and other observational data available from the JCMM through the aegis of the Universities Weather Research Network UWERN.** Plus supplement.
Peter Panagi and Ed Dicks
June 1997

70. **Contributions of the JCMM/Dept of Meteorology Radar Group to 28th AMS Radar Meteorology Conference.** Austin, Texas, September 1997

71. **Sensitivity of short-range weather forecasts to local potential vorticity modifications**
Meral Demirtas and Alan Thorpe
July 1997

72. **Objective identification of frontal wave cyclones**
T D Hewson
August 1997

73. **Attribution and its application to mesoscale structure associated with tropopause folds**
A J Thorpe
September 1997

Met Office Joint Centre for Mesoscale Meteorology Department of Meteorology
University of Reading PO Box 243 Reading RG6 6BB United Kingdom
Tel: +44 (0)118 931 8425 Fax: +44 (0)118 931 8791
www.metoffice.com